

AD-A265 664



2

CERAMIC ACTUATORS FOR SMART MATERIALS

Period 1 July 1991 to 30 June 1992

DTIC
ELECTE
JUN 11 1993
S A D

FINAL REPORT

OFFICE OF NAVAL RESEARCH
Contract No. N00014-91-J-1922

APPROVED FOR PUBLIC RELEASE - DISBRIBUTION UNLIMITED

Reproduction in whole or in part is permitted for any purpose
of the United States Government

L. Eric Cross

PENNSTATE



THE MATERIALS RESEARCH LABORATORY
UNIVERSITY PARK, PA

93 6 10 035

93-13067



REPORT DOCUMENTATION PAGE

Form Approved
OMB No 0704-0188

Public reporting burden for this collection of information is estimated to average 1 hour per response, including the time for reviewing instructions, searching existing data sources, gathering and maintaining the data needed, and completing and reviewing the collection of information. Send comments regarding this burden estimate or any other aspect of this collection of information, including suggestions for reducing this burden, to Washington Headquarters Services, Directorate for Information Operations and Reports, 1215 Jefferson Davis Highway, Suite 1204, Arlington, VA 22202-4302, and to the Office of Management and Budget, Paperwork Reduction Project (0704-0188), Washington, DC 20503.

1. AGENCY USE ONLY (Leave blank)	2. REPORT DATE	3. REPORT TYPE AND DATES COVERED	
4. TITLE AND SUBTITLE CERAMIC ACTUATORS FOR SMART MATERIALS		5. FUNDING NUMBERS	
6. AUTHOR(S) L. ERIC CROSS		8. PERFORMING ORGANIZATION REPORT NUMBER N00014-91-J-1922	
7. PERFORMING ORGANIZATION NAME(S) AND ADDRESS(ES) MATERIALS RESEARCH LABORATORY THE PENNSYLVANIA STATE UNIVERSITY UNIVERSITY PARK, PA 16802		10. SPONSORING / MONITORING AGENCY REPORT NUMBER	
9. SPONSORING / MONITORING AGENCY NAME(S) AND ADDRESS(ES) OFFICE OF NAVAL RESEARCH CODE 1513:RAR 800 NORTH QUINCY STREET ARLINGTON, VA 22217		DOUGLAS E. HEATON DEPT. NAVY/ONR, RES. REP. THE OHIO STATE UNIV. RES. CTR. 1960 KENNY ROAD COLUMBUS, OH 43210-1063	
11. SUPPLEMENTARY NOTES			
12a. DISTRIBUTION / AVAILABILITY STATEMENT		12b. DISTRIBUTION CODE	
<p>13. ABSTRACT (Maximum 200 words)</p> <p>This report delineates work carried out over the period 1 July 1991 to 30 June 1992 on Grant No. N00014-91-J-1922 entitled "Ceramic Actuators for Smart Materials." Two topics were tackled on the program at Penn State.</p> <p>(I) In earlier studies a number of phase switching systems had been explored which permit the switching of large electric polarization and the associated high elastic strain. The question to be resolved was whether these large polarization values could be repeatedly switched without associated mechanical or electrical fatigue. Early fatigue was shown to be an electrode problem and with care in electrode application, density control, grain size control and field homogeneity it was shown that full switching lifetimes with no fatigue of more than 10^9 cycles were achievable.</p> <p>(II) In polymer-ceramic composite transducers the 1:3 type connectivity is highly desirable. A new theoretical approach has been made to calculate the inhomogeneous stress profiles in both piezoceramic and polymer phases. The predictions have been tested using the MRL ultradilatometer and good agreement is shown between predicted and observed strain profiles. A new type of 1:3 composite making use of radially poled ceramic tubes has been explored and shown to offer unusually attractive possibilities for the control of piezoelectric, elastic and electric impedance characteristics and to offer a vehicle for the new electrostrictive agile piezoelectrics.</p>			
14. SUBJECT TERMS		15. NUMBER OF PAGES	
		16. PRICE CODE	
17. SECURITY CLASSIFICATION OF REPORT	18. SECURITY CLASSIFICATION OF THIS PAGE	19. SECURITY CLASSIFICATION OF ABSTRACT	20. LIMITATION OF ABSTRACT

CERAMIC ACTUATORS FOR SMART MATERIALS

Period 1 July 1991 to 30 June 1992

FINAL REPORT

**OFFICE OF NAVAL RESEARCH
Contract No. N00014-91-J-1922**

APPROVED FOR PUBLIC RELEASE - DISBRIBUTION UNLIMITED

Reproduction in whole or in part is permitted for any purpose
of the United States Government

L. Eric Cross

PENNSSTATE



**THE MATERIALS RESEARCH LABORATORY
UNIVERSITY PARK, PA**

TABLE OF CONTENTS

ABSTRACT	3
1.0 INTRODUCTION	4
2.0 ELECTRICAL FATIGUE IN POLARIZATION SWITCHING ACTUATORS.....	4
3.0 PIEZOELECTRIC COMPOSITES	5
REFERENCES	7

APPENDICES

1. Cross, L. Eric and Qiyue Jiang, "Fatigue Effects in High Strain Actuators," Second Joint Japan-US Conference on Adaptive Structures, Nagoya, Japan (November 12-14, 1992), pp. 723-736. Technomic Publishing, Lancaster, Pennsylvania, Edited by Y. Matsuzaki and Ben K. Wada.

2. Jiang, Qiyue, Wenwu Cao and L. E. Cross, "Electric Fatigue Initiated by Surface Contamination in High Polarization Ceramics," Proceedings of IEEE, ISAF 92, Greenville, South Carolina (August 1992), pp. 107-110. .

3. Cao, Wenwu, Q. M. Zhang and L. E. Cross, "Theoretical Study on the Static Performance of Piezoelectric Ceramic-Polymer Composites with 1-3 Connectivity," J. Appl. Phys. 72 (12), 5814-5821 (1992).

4. Zhang, Q. M., Wenwu Cao, H. Wang and L. E. Cross, "Strain Profile and Piezoelectric Performance of Piezocomposites with 2-2 and 1-3 Connectivities," Proceedings of IEEE, ISAF 92, Greenville, South Carolina (August 1992), pp. 252-254.

5. Zhang, Q. M., H. Wang and L. E. Cross, "Piezoelectric Tubes and Tubular Composites for Actuator and Sensor Applications," J. Mat. Sci (in press).

Accession For	
NTIS - CRA&I	M
DTIC - TAB	LI
Unannounced	C
Justification	
By	
Date	
Availability Codes	
DTIC	Special
A-1	

ABSTRACT

This report delineates work carried out over the period 1 July 1991 to 30 June 1992 on Grant No. N00014-91-J-1922 entitled "Ceramic Actuators for Smart Materials." Two topics were tackled on the program at Penn State.

(I) In earlier studies a number of phase switching systems had been explored which permit the switching of large electric polarization and the associated high elastic strain. The question to be resolved was whether these large polarization values could be repeatedly switched without associated mechanical or electrical fatigue. Early fatigue was shown to be an electrode problem and with care in electrode application, density control, grain size control and field homogeneity it was shown that full switching lifetimes with no fatigue of more than 10^9 cycles were achievable.

(II) In polymer-ceramic composite transducers the 1:3 type connectivity is highly desirable. A new theoretical approach has been made to calculate the inhomogeneous stress profiles in both piezoceramic and polymer phases. The predictions have been tested using the MRL ultradilatometer and good agreement is shown between predicted and observed strain profiles. A new type of 1:3 composite making use of radially poled ceramic tubes has been explored and shown to offer unusually attractive possibilities for the control of piezoelectric, elastic and electric impedance characteristics and to offer a vehicle for the new electrostrictive agile piezoelectrics.

1.0 INTRODUCTION

Work on this short one year program focused upon two topics.

- a. The reliability of polarization switching high strain actuators: Penn State work in this laboratory focused upon the fatigue behavior under pure electrical (stress free) drive conditions.

Samples of simple piezoelectric PZT5, Electrostrictive PMN:PT and phase switching compositions in the $\text{PbZrO}_3\text{:PbTiO}_3\text{:PbSnO}_3$ system were also supplied to Dr. Evans group in Santa Barbara to study the performance under pure mechanical boundary conditions.

- b. Work was continued in cooperation with the ONR Transducer Program upon the derivation and measurement of the performance of the simple 1:3 type piezoceramic:polymer composite and upon a new variation on the 1:3 composite theme making use of tubular radially poled ceramic elements working through piezoelectric d_{31} coefficient.

2.0 ELECTRICAL FATIGUE IN POLARIZATION SWITCHING ACTUATORS

The work on this program followed on from earlier studies by W. Y. Pan, C. Q. Dam, Q. M. Zhang and L. E. Cross on "The Performance of Large Displacement Transducers Based on Electric Field Force Phase Transitions,"¹ and of "Polarization Controlled High Strain Actuators," by L. E. Cross² which suggested that the early fatigue observed in these materials on repeated cycling round the hysteresis loop of P vs E (x_{ij} vs E) was a surface and not a volume effect.

Studies on this program and in cooperation with our ONR Transducer Program have shown:

- (a) That early fatigue after $\sim 10^4 - 10^5$ switching cycles in PLZT 7:68:32 is in fact an electrode problem due to a poor interface between the metal and the ceramic. With sputtered gold or indium:thallium metal electrodes on a properly cleaned surface no fatigue is observed to $\sim 10^9$ cycles.
- (b) For fatigue free performance it is necessary that the sample be pore free and transparent as can be achieved by suitable hot pressing in the PLZT family of compositions. Normal ceramic samples ($\sim 98\%$ density) show a logarithmic fatigue commencing $\sim 10^4 - 10^5$ cycles. This type of fatigue is not permanent and the sample can be rejuvenated by heating above the Curie temperature.

- (c) To avoid catastrophic failure under cycling stress it is also necessary to control the grain size to be less than 5 μ meters. Larger grain ceramics exhibit microcracking at the grain boundaries which rapidly leads to complete mechanical failure.
- (d) For extended life the samples must be excited by uniform electric fields. Limited area electrodes lead to large stress concentrations at the electrode perimeter and again exhibit failure due to cracking.
- (e) For the PLZT family it is possible to chose compositions which exhibit shape memory effects at room temperature or at liquid nitrogen temperature. Phenomena which could be of major importance for the control of large area space based mirror structures.

It must be noted that fatigue effects are completely dependent on the cyclic driving to which the samples are subjected, i.e. there are an infinite family of fatigue lifetimes ranging from the aging behavior under zero drive to the instant failure under breakdown level fields.

For these studies the samples were subjected to AC fields at 60 Hz large enough to drive the polarization to a completely saturated hysteresis loop. This is a much more severe fatiguing drive than is normally for a piezoelectric ceramic and was designed to test the possibility of making reliable high strain systems which could utilize the full strain ($\sim 0.4\%$) associated with complete polarization switching.

A more complete account of these studies is given in Appendices 1 and 2. This work is being continued on alternative support.

3.0 PIEZOELECTRIC COMPOSITES

On this program Dr. Qiming Zhang has cooperated with Dr. Wenwu Cao in a more detailed study of the 1:3 type composite which has been widely exploited in hydrophone and in ultrasonic electromedical applications. The objective was to first derive the inhomogeneous displacement profiles for a single rod or single tube of piezoelectric ceramic in a polymer matrix subjected to uniaxial or hydrostatic stress. From this displacement profiles, the stress concentration in both polymer and ceramic phases is calculated. This analysis demonstrates clearly that only a limited part of the polymer which is close in to the surface of the ceramic contributes strongly to the stress enhancement in the ceramics, and that the induced stress in the ceramic is also higher near the surface. The theoretical results quantitatively predict the performance of a given 1:3 composite and can be used to optimize the design parameters, the ceramic content, the aspect ratio of the rods, the

rod geometry and spacing, resin hardness, etc. for optimum performance. This work is effectively summarized in Appendix 3.

Using the MRL ultradilatometer Qiming Zhang has measured the inhomogeneous strain profiles in both 2:2 and 1:3 connected piezoelectric:polymer composites. The experimental profiles show the expected characteristics and compare well with theoretical prediction both for the 2:2 and the 1:3 cases (Appendix 4).

In the above analyses in all cases the piezoactive phase is poled along the length of the rod and tube, so that under uniaxial stress along the rod the electrical charge is generated through the piezoelectric constant d_{33} . For the case of radial poling of a PZT hollow cylinder or tube used as an element in the 1:3 type composite, the situation is more complex and significantly more interesting.

The effective piezoelectric constant in the radial direction can be 'tuned' by varying the ratio of outer to inner radius of the tube (varying the wall thickness) and can be made positive, negative or zero. In this way it is possible to make a composite transducer with all effective piezoelectric constants of the same sign and thus a transducer with very high hydrostatic sensitivity.

The thin walled tube appears to offer some new and most interesting possibilities for actuation. Since the radial field can be made large at low terminal voltage, and is independent of the thickness of the composite (length of the tube), the electrical impedance can be low. Also, as the ceramic is much stiffer than the polymer, the very thin walled tube has lower longitudinal stiffness so that together with a foamed polymer the mechanical impedance can be made very low to interface with an air load. Further, the high field at low voltage suggests that electrostrictive ceramics could be used and the capability to generate an agile piezoelectric response with very high d_{31} also exploited.

This work is summarized in Appendix 5.

REFERENCES

1. W. Y. Pan, C. Q. Dam, Q. M. Zhang and L. E. Cross, "Large Displacement Transducers Based on Electric Field Forces Phase Transitions in the Tetragonal $(\text{Pb}_{0.97}\text{La}_{0.02})(\text{TiZrSn})\text{O}_3$ Family of Ceramics," *J. Appl. Phys.* 66 (12), 6014-6023.
2. L. E. Cross, "Polarization Controlled High Strain Actuators," First Joint US/Japan Conference on Adaptive Structures, Maui (November 1991). Technomics Publishing, Lancaster, Pennsylvania, 1991, p. 807.

APPENDIX 1

FATIGUE EFFECTS IN HIGH STRAIN ACTUATORS

L. Eric Cross,¹ Qiyue Jiang¹

ABSTRACT

In all ceramic piezoelectric and electrostrictive actuator materials, the basic mechanism coupling electric and elastic properties is electrostriction i.e. the strain x_{ij} is related to the components of the Polarization $P_k P_l$ by the relation:

$$x_{ij} = Q_{klj} P_k P_l$$

where the Q_{klj} are electrostriction constants in polarization notation. For the different piezoelectric and electrostrictive ceramics, P_k and P_l may be made up of combinations of spontaneous and induced polarizations and changes of P can also be effected by both domain and by phase changes. In all perovskite structure based systems however the Q_{klj} are 'proper' constants (not morphic) and do not change widely within a given composition family. Thus it is clear that to achieve large shape change (strain) it is essential to be able to induce large changes in polarization.

We have demonstrated in earlier studies (1)(2) that in Lead lanthanum zirconate titanate (PLZT) family of ceramics at compositions which are in the spin glass phase at room temperature, large polarization changes and large strain changes can be induced by a nano to macrodomain phase change driven by electric field.

For PZLTs, the fatigue effects which occur in all high strain systems and limit the number of useful strain cycles driven are particularly accessible to study. In this work we demonstrate:

- (i) That initial fatigue which occurs in the composition 7 : 68 : 32 at $\sim 10^5$ cycles is due to improper electroding procedures.
- (ii) That in hot pressed transparent ceramics of the same compositions with grain size less than $5 \mu\text{m}$ and no visible pores or micro voids, there is not fatigue for $\sim 10^9$ cycles of strain up to 0.4%.
- (iii) For a similar composition which is not hot pressed and contains a normal ceramic pore distribution (ρ actual/ ρ theoretical ~ 97 to 98%) fatigue sets in at $\sim 10^4$ to 10^5 cycles.
- (iv) In large grain samples, a different failure mechanism occurs due to the development of micro-cracks which evolve into macro-cracks rupturing the sample.

¹Materials Research Laboratory, The Pennsylvania State University, University Park, PA 16802, U.S.A

Different compositions of PLZT and of Lead Magnesium Niobate : lead Titanate solid solution show micro to macrodomain transition down to liquid nitrogen temperature. Evidence for strain and fatigue effects in these materials will also be presented.

(1) INTRODUCTION

To describe the electro-elastic interactions in insulating crystalline dielectric materials it is customary to use the phenomenological equations involving the piezoelectric and electrostrictive deformations induced by electric fields in the form

$$x_{ij} = s_{ijkl}X_{kl} + d_{mij}E_m + g_{mnij}E_mE_n \quad (1)$$

where x_{ij} are components of the induced strain
 X_{ij} components of the applied electric field
 E_mE_n components of the applied electric field
 s_{ijkl} the elastic compliance tensor
 d_{mij} the piezoelectric tensor
 g_{mnij} the electrostriction tensor.

In simple linear dielectrics, alternative forms may be written transposing stress and strain, polarization and field and all constants are related by simple transformations. For the nonlinear ferroelectric related dielectrics which are essential for achieving high strain behaviour the relation between E and P is highly nonlinear, often hysteretic and the "constants" d_{mij} and g_{mnij} are strong functions of both field and temperature. In such materials systems it is simpler to describe the elasto-dielectric behaviour using

$$x_{ij} = s_{ijkl}X_{kl} - b_{mij}P_m - Q_{mnij}P_mP_n \quad (2)$$

where P_m, P_n are components of electric polarization
 b_{mij} the piezoelectric tensor now in polarization notation
 Q_{mnij} the electrostriction tensor again in polarization form.

In both equations (1) and (2) the Einstein summation convention is assumed. For (2) however, the coefficients b and Q are now found to be largely independent to temperature and to have similar values in the same structure families.

For bulk samples, the polarization levels which can be induced by realizable electric fields below dielectric breakdown are such that even in very high permittivity ferroelectric or paraelectric dielectrics the constants b and Q do not permit the induction of strains much above $3 \cdot 10^{-4}$. In ferroelectric crystals however, spontaneous polarizations occur which are order to magnitude larger and in some cases induce strain $\sim 1.5 \cdot 10^{-1}$.

In looking for new electro-elastic actuators which can control strains much larger than conventional piezoelectric and electrostrictive ceramics it is then natural to look for materials in which P_s the spontaneous polarization can be controlled.

In earlier studies (1)(2) two different types of phase switching actuators were demonstrated.

- Systems which could be switched by electric field from antiferroelectric ($P=0$) to strongly ferroelectric ($P = P_s$) inducing strains up to 0.8%.

- Compositions in the lead lanthanum zirconate titanate (PLZT) family which settle into a spin glass state ($P = 0$) at the working temperature, but can be switched to a ferroelectric state ($P = P_s$) which induced strains up to 0.5%.

For all ferroic systems, whether ferroelectric, ferroelastic (shape memory) or ferromagnetic where large strains are switched by inducing or reorienting spontaneous strain, there must be concern as to possible mechanisms which may degrade performance on repeated actuations, problems which may stem from a number of different causes but are often lumped together under the heading of fatigue.

It is the purpose of this paper to summarize work on fatigue mechanisms in high strain phase switching actuators which has been carried on the Materials Research Laboratory at Penn State over the last four years.

(2) STUDIES OF FATIGUE IN PLZT PHASE SWITCHING CERAMICS

Previous studies of high strain actuators have explored compositions in the PLZT system chosen near to the morphotropic phase boundary. In describing the PLZT compositions it has become conventional to use the notation X/Y/Z where Y/Z is the ratio of the mole fraction of zirconia to titania, and x is the mole fraction of Lanthanum substituted into the solid solution. Thus for example on 9/65/35 composition has 65% Zirconia to 35% titania with 8 mole% of Lanthanum added. For the compositions explored the maximum switchable strain was over 0.5%. The strain vs field relation is hysteretic, but the strain levels induced are strictly proportional to the square of the inducing polarization. Thus, by current control it is possible to "dial" a specific displacement and the actuator can be left remanent at any chosen strain level. Compositions and dielectric and strain data from the earlier study (2) are listed in Table 1 and the compositions identified on the phase diagram in figure 1.

In any study of the mechanical properties of ceramics at high strain levels, the flaw population which may initiate mechanical failure is critical since the PLZTs can be hot pressed to very near theoretical density and good optical transparency, indicating the complete absence of larger scattering centers with dimensions near to the wavelength of light, they appear to be an ideal vehicle for fatigue studies. With the close correspondence between polarization and induced strain, strain fatigue may be monitored by continuous observation of the polarization levels and only needs to be checked at intervals along the degradation curve.

Initial studies using a 7:68:32 PLZT compositions were however most disappointing (fig. 2) with the material showing severe fatigue after only some 10^4 cycles. A first question which must be answered is whether the fatigue is a surface or a volume phenomenon, does it occur at the electrode:ceramic interface or is it distributed through the volume of the sample. The simple experiment shown in figure 3 answered the question unequivocally for this initial fatigue. For the experiment a square cross section sample rod was cut from the transparent ceramic, polished and cleaned and silver electrodes applied to all surfaces. To separate the major surfaces the edges were beveled leaving two orthogonal electrode pairs (1:2 and 3:4 in fig. 2). With switching field applied between the 1:2 pair polarization was degraded following the curve in figure 3b. The field was then transferred to the 3:4 pair, now clearly if degradation is a volume effect the 3:4 field will be seeing already degraded material, however figure 3c shows that the 3:4 electrodes repeat almost exactly the degradation cycle observed with 1:2, as if they were starting from virgin material. Clearly the observed fatigue is a surface effect. Switching back to the 1:2 electrode pair the sample is still fatigued, however, removing the electrode and re-applying brings the sample back to the un-fatigued virgin state.

The strong suspicion is that the problem is at the dielectric: electrode interface. Roughening the surface to promote adhesion, polishing or even chemically etching modified but did not radically improve fatigue (fig. 2). A treatment which did however eliminate fatigue up to more than 10^8 switching cycles is illustrated in figure 4. The sample was cleaned ultrasonically, then etched in hot phosphoric acid, rinsed and dried at 500°C for ~ 1 hour (fig. 4a). Etching with air drying (fig. 4b) improved the sample with respect to conventional surface preparation (fig. 4c), but the high temperature heat treatment was essential to eliminate fatigue (fig. 5).

Table 1

Dielectric, Polarization and Strain Data for a Number of Spin Glass to Ferroelectric Phase Switching Composition in the PLZT Family at Compositions Close to the Morphotropic Phase Boundary.

Comp	T_m ($^\circ\text{C}$)	K_m	K_{22}	E_c (kv/cm)	P_r (uc/cm ²)	x_t (10^{-3})	x_l (10^{-3})	x_m/x_t
8/67/33	99	12000	5500	2.6	21	0.81	2.5	0.1
8/65/35*	106	11350	4600	3.6	20	0.82	2.3	0.32
8/63/37	114	11300	4500	4.7	21	0.76	1.9	0.32
7/65/35	130	15000	3000	4.5	28.4	1	3.1	0.7
7/62.5/37.5*	160	16000	2900	5	27.2	1.2	3.7	0.64
7/60/40	172	17000	3000	6.3	26.2	1.2	3.8	0.4
7/58/42	180	17300	2600	8	22	1.1	3.2	0.39
7/56/44	190	17200	2200	10	22	0.94	2.3	0.4
6/62/38	196	19000	2100	5	31	1.45	4.1	0.58
6/60/40*	204	18000	2000	5.6	29.5	1.35	4.7	0.57
6/58/42				7.45	29	1.32	3.9	0.53
5/60/40	230	19000	1600	6.52	32	0.79	4.2	0.53
5/58.5/41.5*				6.41	34	1.24	4.5	0.59
5/56/44				8.5	32.1	1.6	5.4	0.56
4/57/43*				7.47	35.2	1.26	3.0	0.6
4/55/45				10	29.5	1.21	2.9	0.55

* MPB compositions: x_t : Transverse strain induced at 15 kv/cm, x_l : Longitudinal strain induced at 15 kv/cm, x_m : Transverse remnant strain, T_m : Temp. of dielectric maximum, K_m : Maximum dielectric constant, K_{22} : Dielectric constant at 25°C .

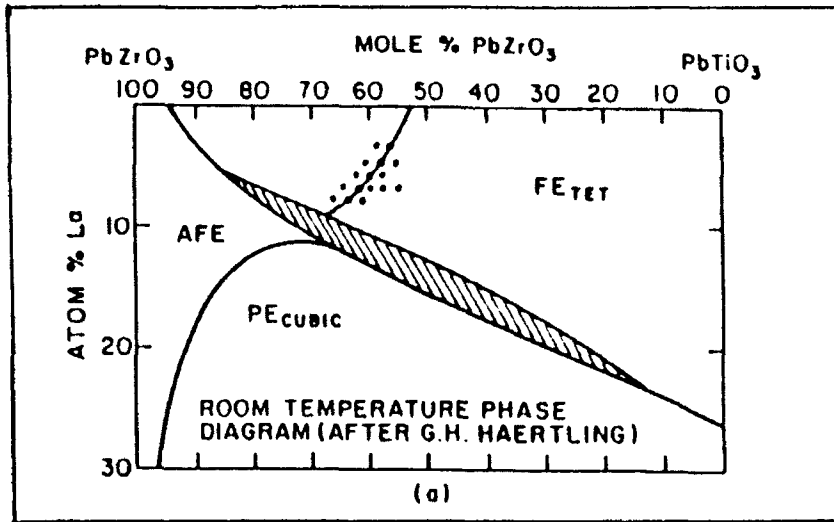


Fig. 1 Identification on the PLZT composition phase diagram of the compositions with properties summarized in Table I. Dots on the diagram indicate the compositions studied.

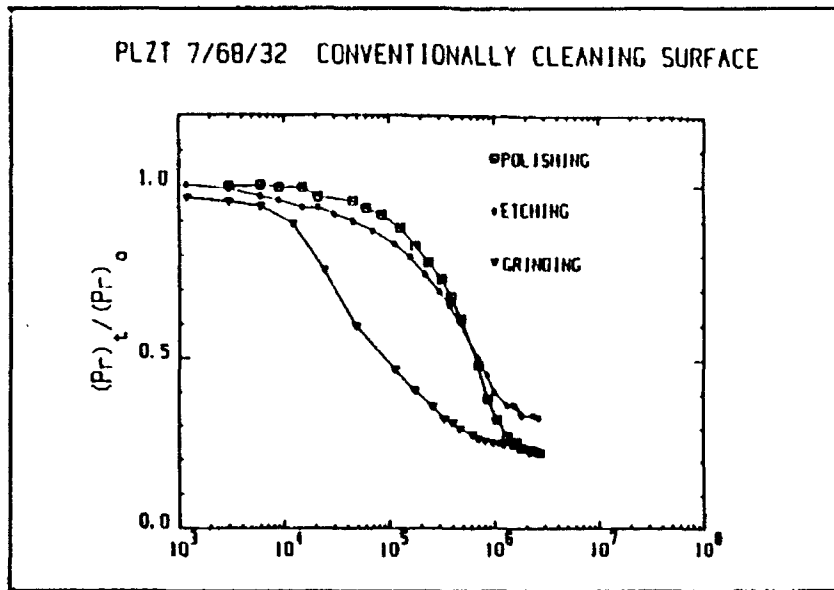


Fig. 2 Early fatigue data for a hot pressed transparent 7/68/32 PLZT composition using sputtered gold electrodes deposited upon polished, etched or ground surfaces after conventional cleaning with organic solvents and distilled water.

That the degradation effect is associated with a surface impedance is suggested by weak field dielectric studies. Using an 8.4/65/35 composition which has a very high dielectric permittivity near 90°C Qiyue Jiang has shown that on thinning a conventionally prepared sample the effective peak permittivity appears to decrease figure 6: just the effect to be expected if there is a capacitive series impedance. If however the electrode is applied immediately after appropriate heat treatment, there is no change in apparent peak permittivity down to less than half the thickness of the conventionally prepared sample (fig. 7).

A most important question concerns the possible role of the high perfection of the hot pressed transparent ceramic. To test the importance an almost identical 7/65/35 composition was prepared by conventional sintering ~97-98% theoretical density, yielding the normal opaque ceramic body. Switching studies compared to the hot pressed body now show degradation begins at $10^4 - 10^5$ cycles and is severe by 10^9 cycles (fig. 8) even though identical electroding procedures were used. Studies have shown that this degradation is a volume phenomenon and cannot be restored by reelectroding.

For the hot pressed theoretically dense samples it may be asked whether the ceramic grain size is important in fatigue. The 7:68:32 composition used for the data in figure 4 had a grain size of order 3 μ meters. Heat treating the sample it was possible to grow the grains to ~30 μ meter. Again it appears that severe fatigue is induced by $10^5 - 10^6$ cycles of field (fig. 9).

That the fatigue behaviour is a complex overlay of several competing mechanisms is evident from studies using 8.4:65:35 compositions. Frequently with this composition, even though the induced strain at saturation is less than in the 7:68:32 composition, the ceramic often failed catastrophically by cracking after only some $10^7 - 10^8$ cycles (fig. 10).

(3) LOW TEMPERATURE STUDIES

An interesting potential application for the hysteretic high strain actuator is in precise position control for large space based telescope mirrors. For a completely active system, the power requirements for many banks of position control actuators could be prohibitive. In the phase switching actuator, if the composition is properly designed polarization switching can be very fast, so that banks of actuators could be serviced by a single power supply which would only be required to update the actuator against aging and system drift. For such systems however it would clearly be necessary for the actuator to be in intimate contact with the mirror, whose surface would probably be at space ambient temperature ~100°K, i.e. - 173°C. Thus it is important to know how polarization controlled high strain actuators would behave at low temperature.

In the spin-glass type switching systems it is important to explore the freezing temperature as a function of composition. From such studies which will be reported elsewhere it was clear that the 9.5/65/35 PLZT and pure lead magnesium niobate (PMN) would be adequately square hysteretic. For the PLZT, polarization and strain curves taken at -132°C are shown in figure 11. Clearly strains up to $-2.5 \cdot 10^{-3}$ can be retained remanently in this temperature. Pure PMN at -140°C (fig. 12) has a rather less square hysteresis loop and the strain level is now less than $2 \cdot 10^{-3}$.

In both the PLZT composition (fig. 13) and the PMN (fig. 14) full switching up to 10^7 cycles only leads to very small fatigue. If the actuator were used in a static deflection situation and only updating pulses were applied we believe this level of fatigue would be acceptable for practical situation. Clearly if the actuator has to be continuously exercised across the full strain range further improvement will be necessary.

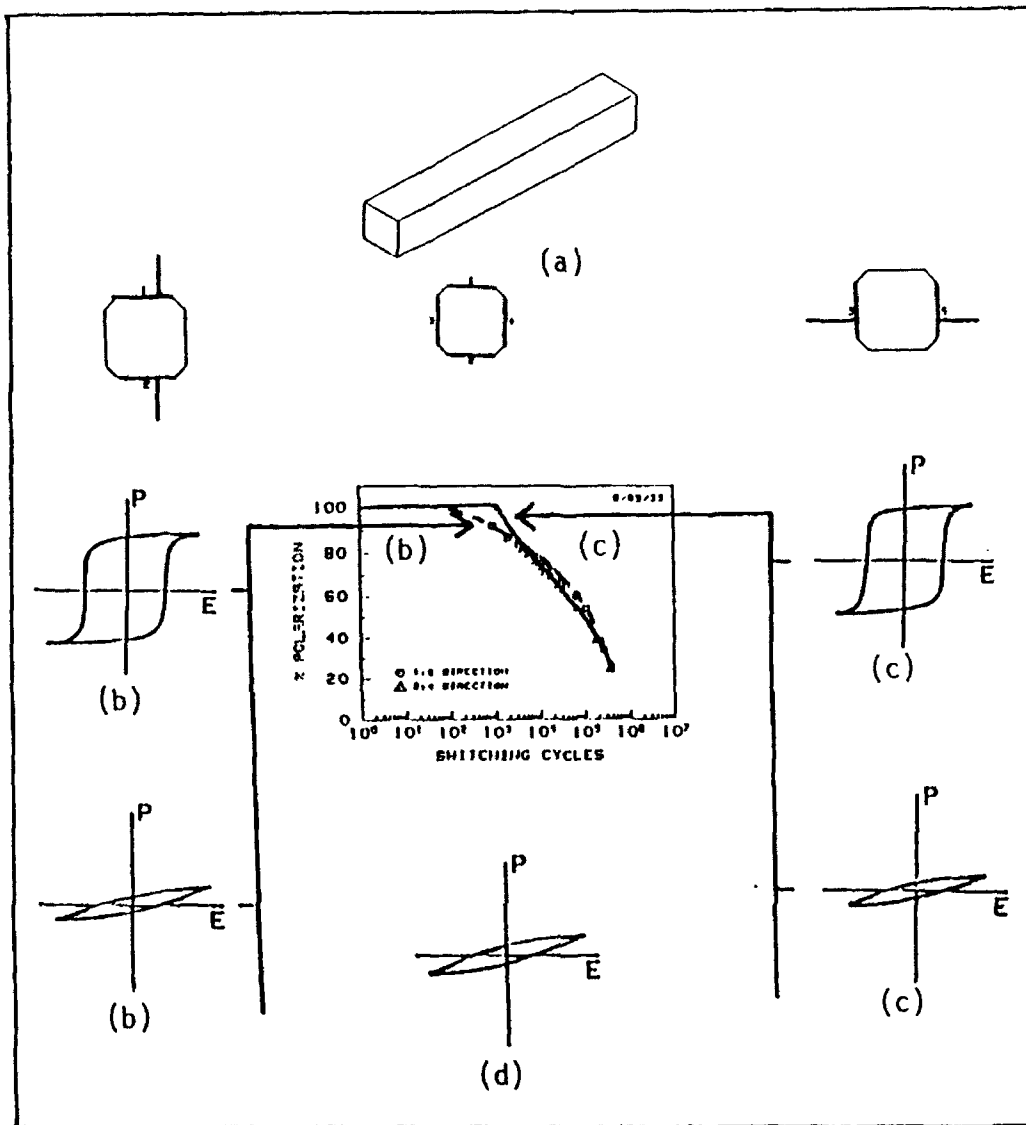


Fig. 3 Experimental configuration used to demonstrate that early fatigue is a surface not a volume related problem.

- (a) Square cross section sample of 8.4/65/35 PZT electroded on the major surfaces, but with the edges beveled to separate 1:2 and 3:4 electrode pairs.
- (b) Modification of the dielectric hysteresis and polarization degradation for fields in the 1:2 direction.
- (c) Modification of hysteresis and polarization with field cycling for fields in the 3:4 direction. Note that for 3:4 degradation again starts as if for a virgin sample.
- (d) Returning field to either 1:2 or 3:4 electrode pairs after fatigue the sample remains in the fatigued state.

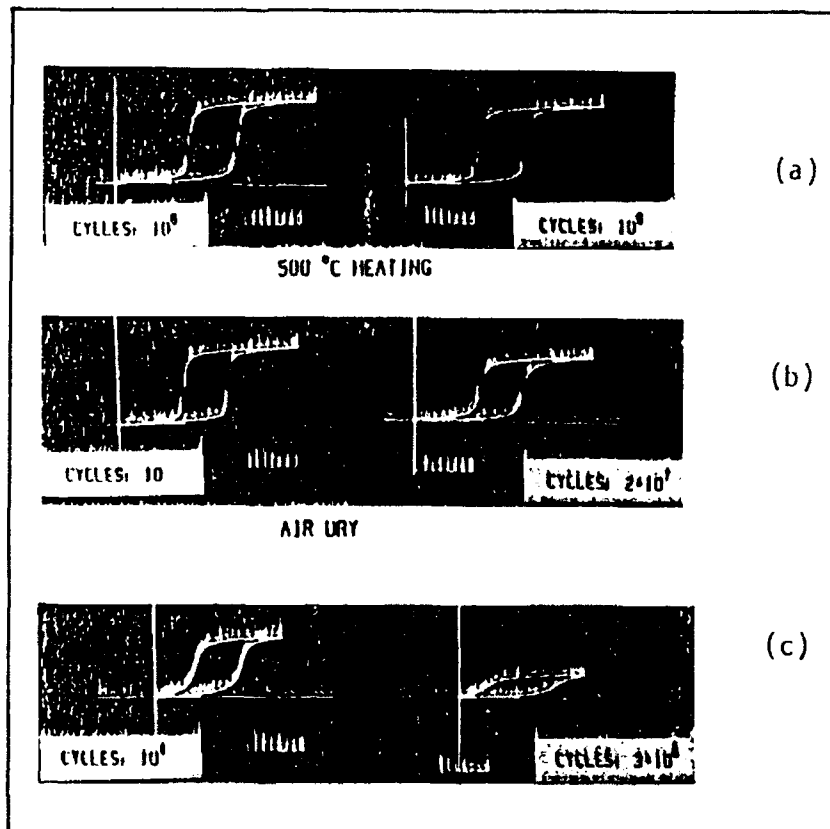


Fig. 4 Hysteresis behaviour showing the effects of different surface treatments on a hot pressed transparent 7:68:32 PLZT before sputter deposition of gold electrodes.

- (a) For maximum resistance to fatigue the treatment involves etching in hot phosphoric acid, rinsing in distilled water then heat treating to 500°C for one hour immediately before electrode deposition.
- (b) Fatigue evident at $2 \cdot 10^7$ cycles after phosphoric acid etch, rinsing and drying without heat treatment.
- (c) Severe fatigue associated with electrodes applied to conventionally prepared PLZT surfaces.

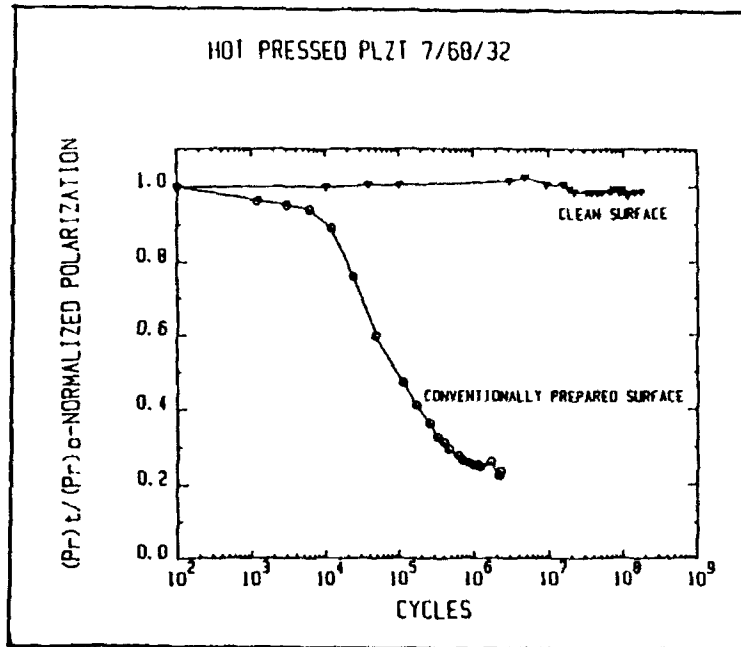


Fig. 5 Comparison of fatigue life for a PLZT 7:68:32 composition with etched and heat treated surfaces and with conventionally prepared surfaces.

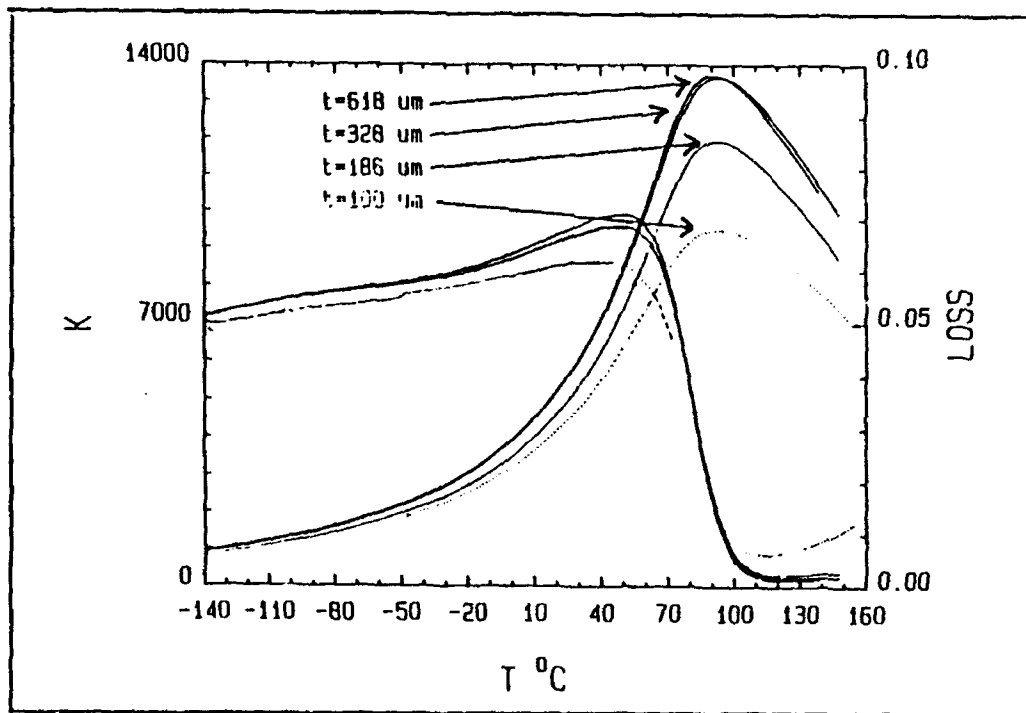


Fig. 6 Weak field dielectric permittivity as a function of temperature in 8 -4/65/35 PLZT with polished and conventionally cleaned surfaces as a function of sample thickness. Note that at 100 μm thickness there is severe degradation of the apparent peak permittivity due to series capacitive impedance.

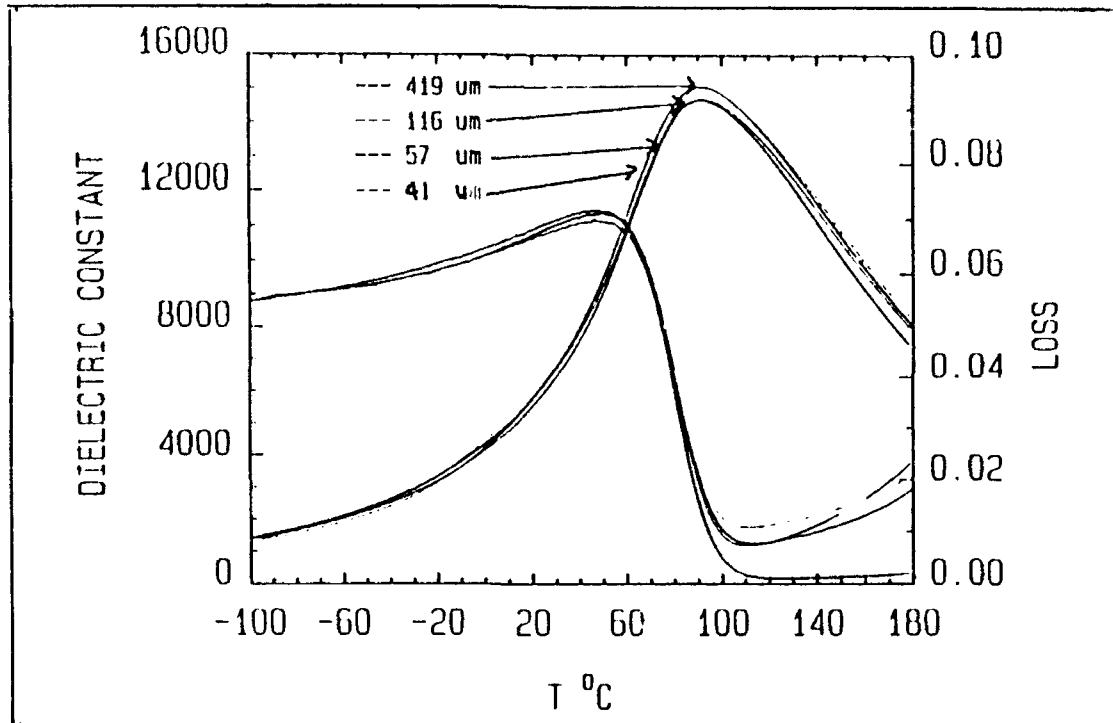


Fig. 7 Weak field permittivity of a similar 8.4:65:35 PLZT composition with etched heat treated surfaces. Note that there is no evidence of a series impedance at the surface for samples down to 41 μm thick.

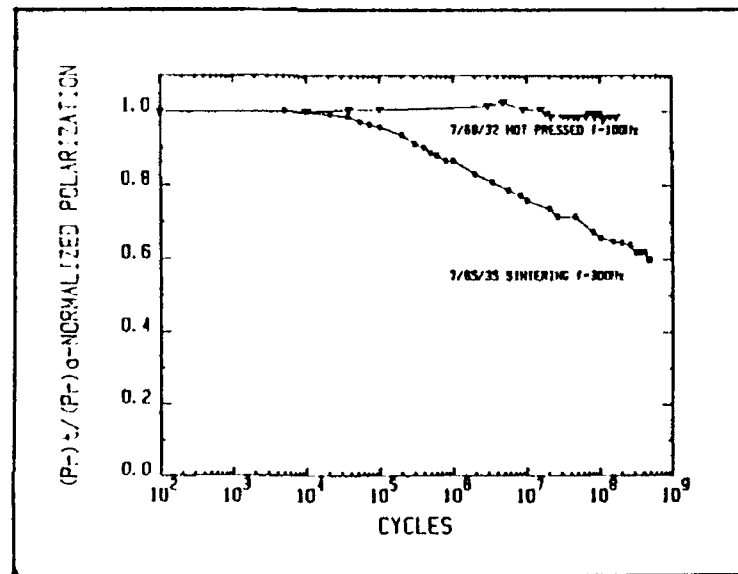


Fig. 8 Comparison of the fatigue behaviour between hot pressed theoretically dense 7:68:32 and a conventionally sintered 7:65:35 composition. Curves were taken using the same electrode treatments. Damage in the 7:65:35 compositions could not be rejuvenated by re-electroding and appeared a volume phenomenon.

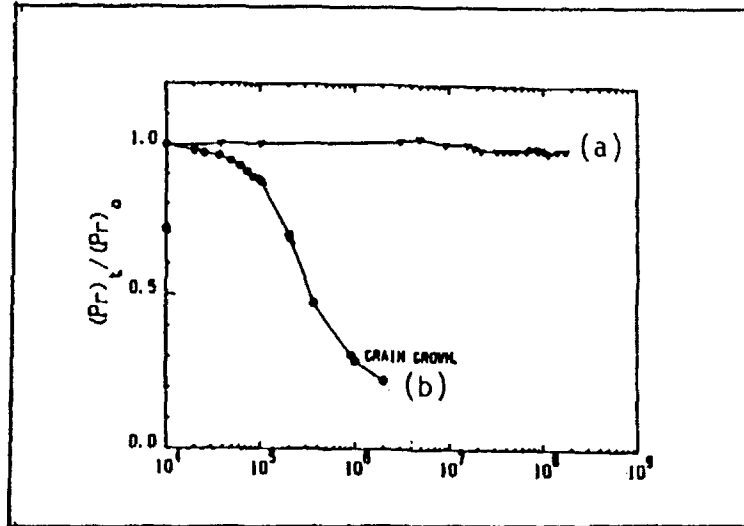


Fig. 9 Effects of ceramic grain size on fatigue (a) 7/68/32 PZT with grain size ~3 μmeters; (b) 7/68/32 PZT grain grown to size ~30 μmeters.

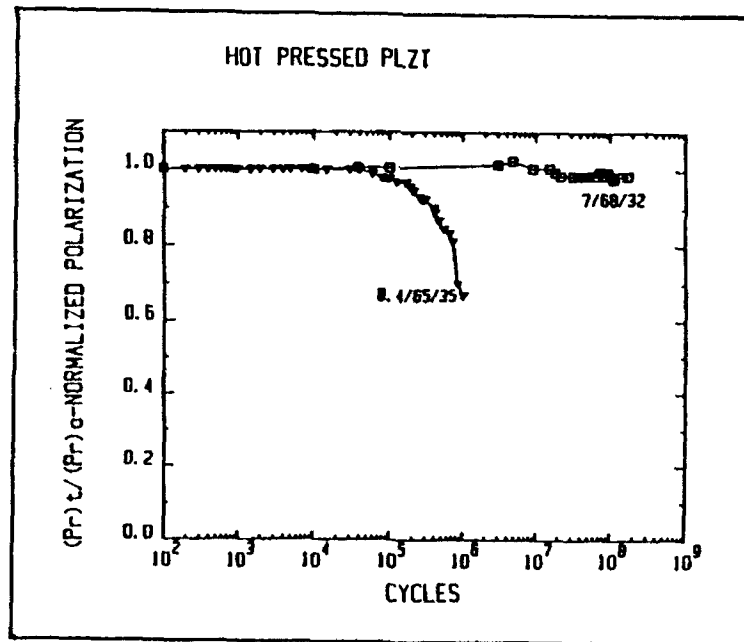


Fig. 10 Fatigue in a 7/68/32 composition as compared to that in an 8-4/65/35 composition. Note that the 8-4/65/35 undergoes lower strain excursions than the 7/68/32 composition, but though it has similar grain size and the same electrode treatment it falls catastrophically by cracking after only 10^6 cycles.

(4) SUMMARY AND CONCLUSIONS

For high strain phase switching actuators based upon spin glass like compositions in the PLZT family it has been shown that the fatigue effects which limit the number of useful strain switching cycles involve a number of phenomena.

For hot pressed theoretically dense optically transparent ceramics, the electrode structure has been shown to be critical if premature fatigue is to be avoided. For sputtered gold electrodes, etching in phosphoric acid followed by a high temperature heat treatment immediately before electrode application was shown to yield fatigue free performance up to 10^9 cycles. Conventional ceramics of ~97-98% theoretical density made by conventional sintering could not be made fatigue free. The grain size and the composition of the ceramic were also shown to play a major role in determining the lifetime. In general finer grain ceramics as expected had longer fatigue lifetimes, however composition is a more sophisticated variable and failure does not appear to be directly keyed to strain performance.

Initial low temperature studies have shown that hysteretic (dial-a-displacement) actuators can be developed to work at temperatures ~-140°C. Fatigue at 10^7 cycles is quite small and for simple updating to maintain a near constant static displacement present materials will be quite adequate.

In many high strain applications it will be necessary to use multilayer systems with cofired electrodes so as to achieve adequate displacements at low terminal voltages. It will be important to repeat these types of fatigue studies for system with cofired internal electrodes.

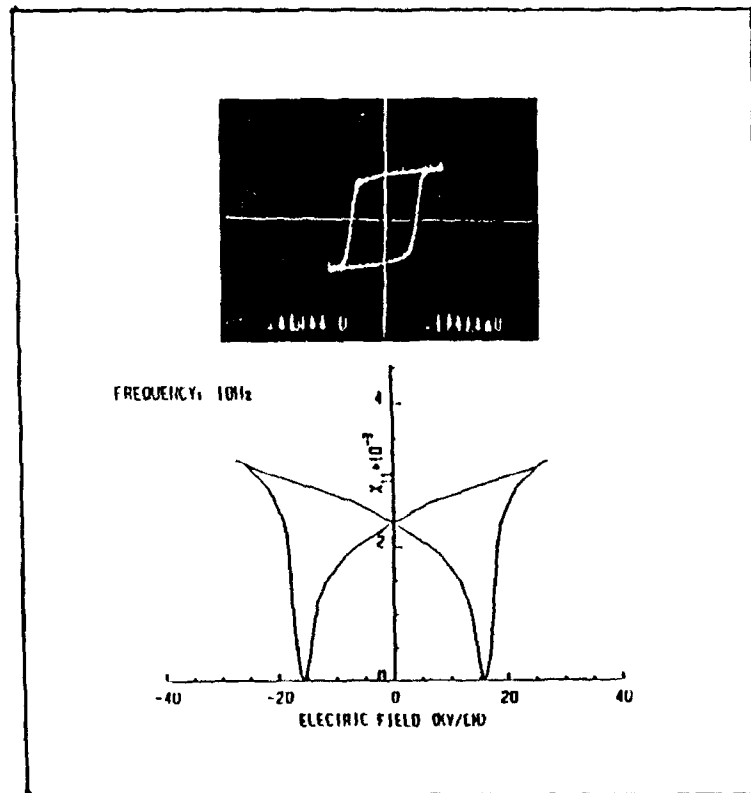


Fig. 11 Low temperature polarization and strain cycles in a 9.5/65/35 PLZT. Frequency 10 Hz, Temperature -132°C, Cycling field 30 KV/cm.

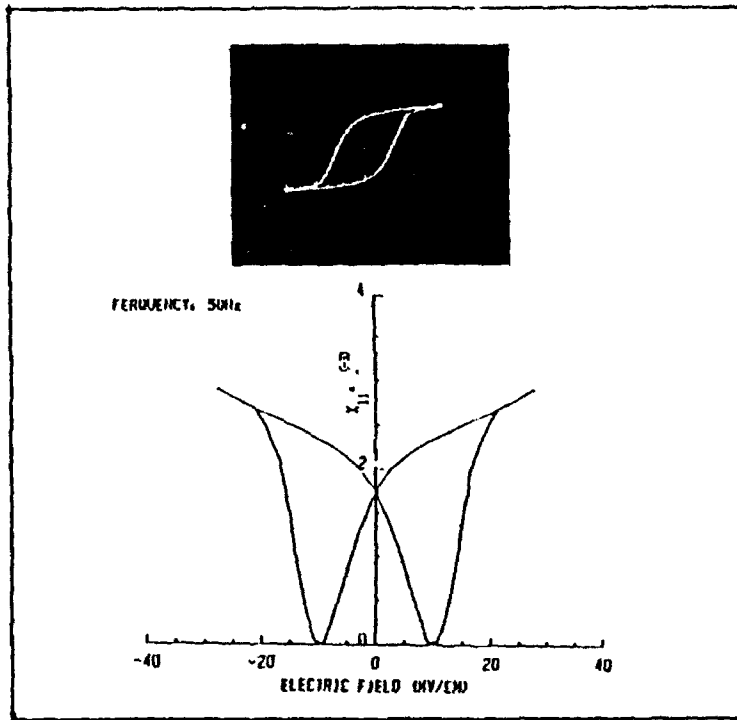


Fig. 12 Low temperature polarization and strain curves in pure Lead magnesium niobate (PMN).

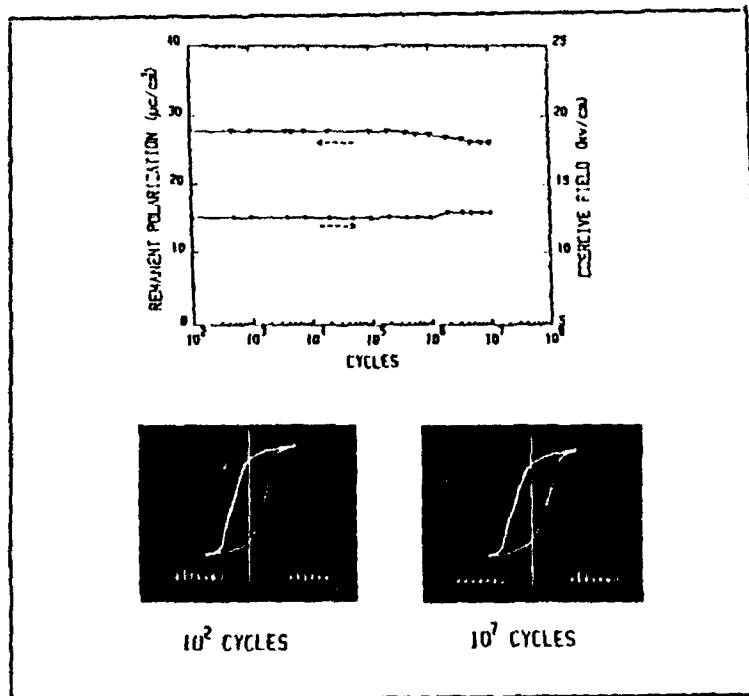


Fig. 13 Fatigue in the 9.5/65/35 PLZT under high field cycling under a frequency of 160 Hz at -140°C .

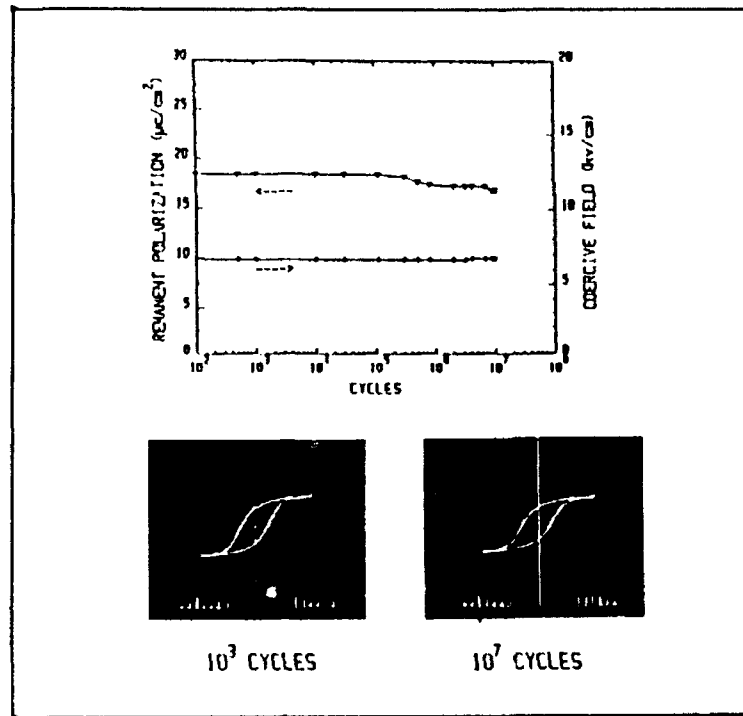


Fig. 14 Fatigue in pure PMN under high cyclic field of 100 Hz applied at -140°C .

REFERENCES

1. W. Y. Pan, C. Q. Dam, Q. M. Zhang and L. E. Cross. "Large Displacement Transducers based on Electric Field Forced Phase Transitions in the Tetragonal $(\text{Pb}_{0.97}\text{La}_{0.02})(\text{Tl}, \text{Zr}, \text{Sn})\text{O}_3$ Family of Ceramics," *J. Appl. Phys.* **66** (12), 6014-6023 (1989).
2. L. E. Cross. "Polarization Controlled High Strain Actuators." First Joint US:Japan Conference on Adaptive Structures. Editors B. K. Wada, J. L. Farson, K. Miura, Technomic Publishing, Lancaster (1991), p. 807.

APPENDIX 2

ELECTRIC FATIGUE INITIATED BY SURFACE CONTAMINATION IN HIGH POLARIZATION CERAMICS

Qiyue Jiang, Wenwu Cao and L. E. Cross
Materials Research Laboratory
The Pennsylvania State University
University Park, PA 16802

ABSTRACT

Recently electric fatigue phenomenon in high polarization ceramics has attracted more and more attention because of the development of high strain actuators and ferroelectric memory devices. We report a study on fatigue behaviors of hot pressed PLZT with composition 7/68/32 under different surface conditions. It is found that the fatigue occurred at a few thousand of cycles is mainly caused by contaminated surface instead of intrinsic structure deterioration. For the same gold electrodes, samples with conventionally cleaned surface showed significant fatigue within 10^5 switching cycles while samples with surfaces cleaned by an improved procedure did not fatigue even after 10^8 switching cycles. The mechanism of fatigue introduced by surface contamination is explained by interface degradation between ceramic and electrode.

INTRODUCTION

Many applications of high polarization ceramics, such as high strain actuators and ferroelectric memory devices, involve repeated reversals of the polarization. One critical limitation on the performances of these devices is the fatigue associated with repeated electrical cycling.

In 1953, McQuarrie [1] first reported the time dependence of the P-E hysteresis loop in a BaTiO₃ ceramic. He found that after several weeks of switching at 60 Hz, the square shaped hysteresis loop was changed to a distinct propeller shape with some obvious decrease in both the maximum polarization and the remnant polarization. Merz and Anderson [2] studied fatigue behavior in a single BaTiO₃ crystal, a gradual reduction of polarization after a few million switching cycles was observed and the fatigue behavior was related to the patterns of the electric field (sine wave or pulse train wave). The ambient atmosphere was also reported to affect on the switching stability of BaTiO₃ single crystal [3]. A more detailed study of fatigue was carried out by Stewart and Cosentino on La or Bi doped PZT ceramics [4], they showed that the polarization decreased rapidly and was reduced to half of its original value after 5×10^9 switching cycles. They concluded that the patterns of electric field, the types of electrodes, and the ambient conditions had no significant effects on the fatigue behavior. Fraser and Maldonado [5] also studied the same La doped PZT ceramics and reported significant effects of the electrodes. They found that when indium was used as electrode material instead of gold or silver, there was still 85% of the original remnant polarization left after 10^9 switching cycles, but fatigue occurred much faster when using lead, aluminum, gallium, silver and gold as electrode material. Carl [6] observed significant degradation in the La or Mn doped PbTiO₃ ceramics, after only a few thousand switching cycles the polarization dropped to 30% of its original value together with some increase of the coercive field, and some cracks were also observed on the surfaces of the samples under SEM.

Despite the fact that the fatigue effect is the major factor which prevents some potential applications of ferroelectrics, only a limited number of papers have been published on this subject. In addition, these published results by different investigators are often in contradiction, and there are no satisfactory explanations for these discrepancies. Therefore a systematic study on this subject is needed in order to understand the origin and mechanism of fatigue behavior. We report here the first part of an extensive study of the fatigue behavior on La doped lead zirconate titanate (PLZT) ceramic system. The reason for choosing PLZT ceramic system is because its relatively low coercive field, large polarization and square shaped hysteresis loop. Moreover, hot pressed PLZT ceramics are transparent, therefore have potential applications in non-volatile memory, electro-optical, and electrostrictive devices. In this paper, the focus will be on the effect of surface contamination on the fatigue behavior. We believe that different surface conditions was one of the

main reasons for the inconsistencies of those reported experimental results.

EXPERIMENT PROCEDURES

Lanthanum doped lead zirconate titanate ceramic specimens were fabricated from mixed oxides by hot pressing technique. The composition used in this study is $\text{Pb}_{0.93}\text{La}_{0.07}(\text{Zr}_{0.68}\text{Ti}_{0.32})_{0.9825}\text{O}_3$. Conventionally, this formula is simplified to a form 7/68/32 according to the mole ratio of La/Zr/Ti. The average grain size is about 5 μm . At room temperature 7/68/32 is in rhombohedral phase. Samples were first cut into platelets with the areas of about 10 mm² and thicknesses in the range of 150-300 μm , then annealed at 600 °C for 1 hour to release the mechanical stress generated during cutting and grinding processes.

In conventional cleaning procedure, organic solvents (alcohol or acetone) were used to rinse the samples and then the samples were dried in air at room temperature. An improved cleaning method used in our experiments is described as follows: first the samples are cleaned by conventional procedure, then they are further cleaned ultrasonically in solvent, and finally the samples are heated in a furnace for 1 hour at 500-600 °C. Gold electrodes were sputtered onto the sample surfaces.

The properties studied here are the remnant polarization P_r , the maximum polarization P_m , coercive field E_c , and the dielectric constant in depoled state. High voltage sine wave AC field was used to switch the polarization, and the hysteresis loops were measured through a conventional Sawyer-Tower circuit and a Nicolet 214 digital oscilloscope.

RESULTS AND DISCUSSION

Fatigue in PLZT Specimens Cleaned by Conventional Procedure

Fig. 1 shows a typical result obtained at 10 Hz from a specimen cleaned by conventional procedure. One can see that the fatigue started at about 10^3 switching cycles, and proceeded very rapidly between 10^5 - 10^6 cycles. The polarization P_r dropped to a value below 30% of the initial values after 10^6 switching cycles. The changes of the saturated polarization which was not show here have similar behavior as that of the remnant polarization P_r . Fig. 2(a) and 2(b) are typical hysteresis loops before and after the fatigue test. The coercive field E_c also increased with switching cycles. We found that the polarization decrease is always accompanied by the increase of the coercive field E_c , which is consistent with the results obtained by other researchers [4][5][7]. Measurements made at the frequencies of 100 Hz and 200 Hz did not show apparent difference.

Fatigue in PLZT Specimens Cleaned by Improved Procedure

Fig. 3 shows the changes of the polarization and coercive field with switching cycles for samples cleaned by improved procedure. The experiment was carried out at a frequency of 100 Hz. No fatigue was observed even after 10^8 switching cycles. We can see this more clearly from the two hysteresis loops in Fig. 4, which were recorded at 10^3 and 2×10^8 switching cycles, respectively. We can conclude from these experimental results that the fatigue shown in Fig. 1 is purely extrinsic, i.e., caused by dirty surfaces. The actual lifetime of PLZT 7/68/32 ceramics with average grain size 5 μm is much longer than that shown in Fig. 1. For improperly cleaned samples, the organic contaminants are trapped at the ceramic-electrode interfaces. During switching, a large electric field (15-40 kV/cm) was continuously applied on the sample, the trapped contaminants will cause large field concentrations resulting a failure of the electrode bonding.

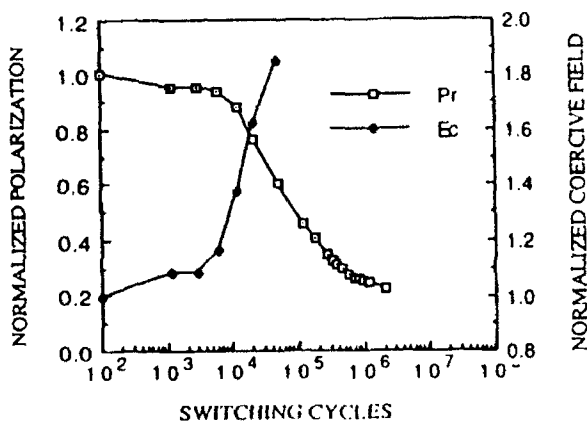


Fig. 1 The changes of the normalized remnant polarization P_r and coercive field E_c with switching cycles for a conventionally cleaned PLZT 7/68/32 specimen.

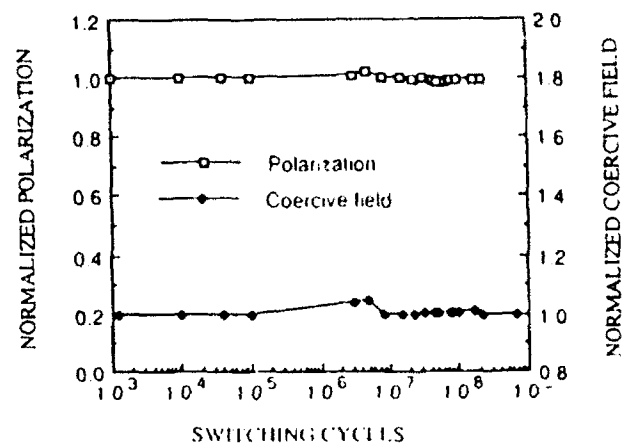


Fig. 3 The normalized polarization and coercive field as functions of the switching cycles for a specimen cleaned by the improved procedure.

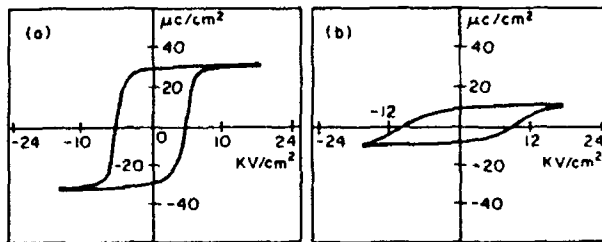


Fig. 2 Typical hysteresis loops at 10^3 (a) and 3×10^6 (b) switching cycles for a conventionally cleaned PLZT 7/68/32 sample at a frequency of 10 Hz.

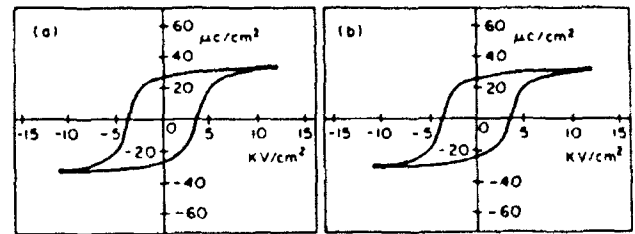


Fig. 4 Typical hysteresis loops of a sample cleaned by improved procedure at a frequency of 100 Hz. (a) at 10^3 switching cycles, and (b) at 2×10^8 cycles.

Although these experimental results may not be used as a proof to discredit the validity of other previous explanations on fatigue in terms of internal domain behavior, we can at least conclude that the fatigue in fine grain hot pressed PLZT 7/68/32 is caused by the improper ceramic-electrode interface, may be eliminated through an improved cleaning procedure described above. This finding is encouraging for many prospective applications of ferroelectrics.

Fatigue Originated from Surface Contamination

A. Deterioration of Ceramic-Electrode Interface under High AC Field

In fatigue experiments the possible sources of contaminants are: abrasive residue from grinding process; residue of solvents (water, alcohol or acetone); water in the air; residue of the bonding glue from cutting process; skin grease from finger touch. Without further cleaning these contaminants are left on the surfaces of specimens, and being sandwiched between the sample surface and the electrode, producing a poor interface contact. The effects of solvents and skin grease were further examined in the following experiments. First, the samples were etched by H_3PO_4 acid to remove the abrasive residues and skin grease, then the following surface treatments were given to three different samples:

- sample 1 was washed by water and acetone, then rubbed both surfaces by fingers;
- sample 2 was washed by water and acetone, then let it dry in the air;
- sample 3 was washed by water and acetone, then heat treated in a furnace at 500 °C for 1 hour (free from contamination).

Fig. 5 shows the results from the fatigue tests on these samples using a 100 Hz sine wave AC field. The remnant polarization of sample 3 did not decrease at all after 10^8 switching cycles, only E_c increased slightly. The P_r of sample 2 fatigued to 85% of its initial

value after 10^8 switching cycles and E_c increased about 18%. Sample 1 was the worst among the three samples, its P_r reduced to 30% of the initial value, and E_c increased 50% after only 2×10^6 cycles. Since the three samples only differ in surface treatments, these discrepancies in fatigue results can only be explained in terms of the different degree of surface contamination.

Although the experiments clearly indicate that the fatigue is initialized at the interface between the surface and electrode. The reactions of organic contaminants under high AC field at the interface are very complicated. A few possible explanations for what might have happened at the interface are: 1) electrochemical reaction, such as ionization of contaminants, reduction of the chemical composition near the sample surface; 2) corona, high voltage can ionize water and organics, causing partial discharge which leads to a time related continuous degradation of the dielectric property; 3) contact deterioration effect, residue of solvents and skin grease prohibit a direct contact of the metal electrode with the sample surface, resulting a poor contact. When a poor contact occurs, a large field is applied to the contaminant layer which has much smaller dielectric constant than the sample, causing electrochemical reaction, resulting in a partial failure of the contact.

The electrode surface of a fatigued sample (which was cleaned by conventional method) was examined under SEM, and many regions were found where the electrode has been separated from the ceramic as shown in Fig. 6. We believe from our experimental observations that the explanation 3) above may be the most appropriate one.

B. The nature of the fatigue by surface contamination

In order to find the nature and degree of damage produced during fatigue, different heat treatments were given to a fatigued sample. Table 1 listed the remnant polarization P_r and the coercive field E_c measured after the fatigued sample went through a heat treatment at 300 °C for 3 hours. Only partial recovery of P_r was

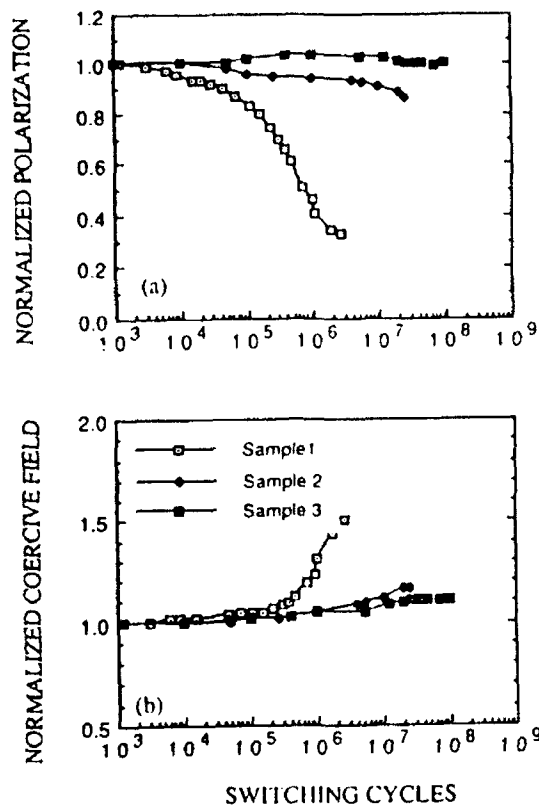


Fig.5 The normalized remnant polarization (a) and coercive field (b) as functions of switching cycles. Sample 1 was contaminated by solvent and skin grease; sample 2 was contaminated by solvent; sample 3 was cleaned by the improved procedure.

Table 4.1 Comparison of the remnant polarization (P_r) and the coercive field (E_c) for a PLZT 7/68/32 sample under different treatments

	P_r ($\mu\text{C}/\text{cm}^2$)	E_c (kv/cm)
Before fatigue	27.0	5.0
After fatigue	6.0	6.8
After 300°C heating	19.2	10.4
After 600 °C heating	22.4	7.3
After removal of 30 μm	22.5	7.2

achieved and E_c became even larger. The sample then experienced further heat treatment at 600 °C for 1 hour, further improvements were observed as shown in Table 1. However, the P_r and E_c still could not recover to their initial values, which means that part of the damage in the fatigued sample is permanent. In order to investigate the depth of the damage from surface initiated fatigue, the sample was then ground off a 15 μm thick layer from each surface and re-electroded. The measured results (table 1) show no further improvement, which indicates that the damage has propagated to the interior of the sample.

Previously, fatigue in ferroelectrics was explained as due to the stabilization of domain walls [1][4][10]. Fatigue caused by domain pinning usually can be recovered by heating the samples to paraelectric phase [4][10]. In our experiments, total recovery did not occur even after the fatigued sample has been heated to as high as 600



Fig.6 SEM photograph taken from the electroded surface of a fatigued sample.

°C which is 470 °C higher than the dielectric maximum temperature. Therefore, the fatigue we have observed could not be due to the domain wall pinning, instead, we believe that the intergranular microcracking is responsible for the non-recoverable fatigue initiated by surface contamination. Scanning Electron Microscopy was performed on a fatigued sample (Fig 7 a) and non-fatigued sample (Fig 7 b) with ground surfaces. The samples were etched using H_3PO_4 acid to remove gold electrodes. On the micrographs in Fig.7, we can see some of the grinding damages and etch-pits for the non-fatigued sample, while for the fatigued sample we see a lot of grains without grinding damages and etch-pits. This means that a whole layer over these grains was pulled out during etching, which indicates that the bonding between grains was weakened during fatigue test. In addition, some cracks around grain boundaries are clearly visible, but no large cracks were observed either on the surfaces or on the cross section of the fatigued sample.

Fig.8 is an optical micrograph which was taken from a fatigued sample after the electrode being carefully removed. Many regions in the original transparent sample become opaque, which indicates that the nonuniform damage in the fatigued sample. This non-uniform damage is due to the partial failure of the electrode caused by the trapped contaminants.

SUMMARY AND CONCLUSIONS

A systematic study has been carried out on the influence of surface conditions on the fatigue behavior of hot pressed PLZT 7/68/32 ceramics with an average grain size of 5 μm . It is found that the observed fatigue which occurred within 10^5 switching cycles is actually caused by surface contamination. These surface contaminants cause deterioration of the contact between the ferroelectric ceramic and the electrode, resulting an inhomogeneous field distribution in the specimen. Microcrackings are generated at the grain boundaries due to high electric field concentration. As a result, the applied field then will be concentrated across those cracks parallel to the electrode, which effectively raise the coercive field and lower the polarization. The conventional cleaning method is proved to be inappropriate for specimens used under high AC field. This surface contamination initiated fatigue can be eliminated through an improved surface cleaning procedure. Our results show that the ferroelectric properties of PLZT 7/68/32, such as the polarization and the coercive field, can be preserved for more than 10^8 switching cycles if the surface contaminants are removed.

Contrary to some reported results [4][10], We found that part of the fatigue damages are permanent and are throughout the entire sample. The fatigued properties i.e., the reduced polarization and the increased coercive field can be partially recovered though heat treatment, however, a complete recovery is not possible.

It should be pointed out that the results obtained here are applicable only for small grain ceramics, the fatigue mechanism in large grain systems is different [11].

APPENDIX 3

Theoretical study on the static performance of piezoelectric ceramic-polymer composites with 1-3 connectivity

Wenwu Cao, Q. M. Zhang, and L. E. Cross

Materials Research Laboratory, The Pennsylvania State University, University Park, Pennsylvania 16802

(Received 6 July 1992; accepted for publication 2 September 1992)

Inhomogeneous displacement profiles have been derived for a single-rod composite and a single-tube 1-3 ceramic-polymer composite under both uniaxial and hydrostatic stress. The effective piezoelectric constants for the composites have been derived in terms of the ceramic content, the piezoelectric and elastic constants of each component, and the aspect ratio of the ceramic rod. The stress concentration inside both phases is derived from the calculated inhomogeneous displacement profiles. It is found that only a finite portion of the polymer in the vicinity of the ceramic-polymer interface actually contributes to the stress transfer, and the induced additional stress on the ceramic also has a higher magnitude near the interface. The theoretical results quantitatively predict the performance of a given 1-3 structure, and can be used to optimize the design parameters, such as ceramic content, aspect ratio of the ceramic rods, rod geometry and rod arrangement, resin hardness, etc., for 1-3 structures designed for specific purposes.

I. INTRODUCTION

With the increasing application of piezoelectric composite structures, quantitative description of their physical properties has become a necessity for proper structural design. The most frequently encountered piezocomposites are 2-2- and 1-3-type ceramic-polymer composites. The names of these composites are defined according to their connectivities.¹ In the past, theoretical studies on this subject have been limited to the isostrain models.²⁻⁴ Although the isostrain models can provide some general guidelines, their theoretical predictions are often larger than the experimental values.⁵ In addition, the effect of the aspect ratio, which is proven experimentally to be a critical parameter in the 1-3 composite structure, is not included in the isostrain models. After analyzing the essential characteristics of the problem we have presented in a previous paper a theoretical model for the 2-2 composites.⁶ This model can quantitatively describe the effective piezoelectric properties of the 2-2-type composites. In this paper we extend the model to address the 1-3-type composites which are more attractive and have much wider applications than the 2-2 structures from a practical point of view.

The fundamental physics in the 1-3 composites is the same as that in the 2-2-type composites. We expect the displacement profile in a 1-3 composite to be inhomogeneous under a prescribed stress field or an electric field because the two components have different elastic and piezoelectric properties. The difference between the 2-2 and 1-3 problems is the dimensionality, i.e., one-dimensional for the 2-2 type and two dimensional for the 1-3 type. Besides the dimensionality difference, there are two more complications in the 1-3-type composites: one is the geometry of the cross section of the ceramic rod, which is commonly chosen to be square or circular due to manufacturing convenience; the other is the rod arrangement in

the composite, which usually is made into square or triangular configurations. Because the rod geometry and the rod arrangement define the boundary conditions for the problem, each case must be treated separately. Here we only solve two simple cases for which analytic solutions exist; using these two examples we wish to derive the essential features of the 1-3 structure and demonstrate the general procedure for dealing with the 1-3 composites. Solutions for an arbitrary rod geometry and rod arrangement may be calculated numerically.

The two cases to be treated are composites made of a single cylindrical ceramic rod and a single ceramic cylinder with a polymer matrix of finite dimension as shown in Figs. 1 and 2, respectively. One can think of them as the "unit cells" of a 1-3 composite. For simplicity, the outer boundary of the composite is also defined to be circular. Obviously, such a unit cell cannot be used to fill the whole space. However, it is a reasonable approximation to the composite with triangularly arranged ceramic rods (for which the unit cell has hexagonal symmetry) and, as will be proven later, at low ceramic content the results for the single-rod composite can even be used for composites with other rod arrangements.

II. DISPLACEMENT PROFILE IN A SINGLE-ROD COMPOSITE UNDER UNIAXIAL AND HYDROSTATIC STRESSES

The basic idea for constructing the static equilibrium condition is to single out the effective component of the displacement field. For the single-rod (tube) system as shown in Fig. 1 (Fig. 2), we choose a cylindrical coordinate system (r, ϕ, z) with the z and r directions along the axis of the ceramic rod (tube) and the radial direction, respectively, and ϕ as the angular variable. When the ce-

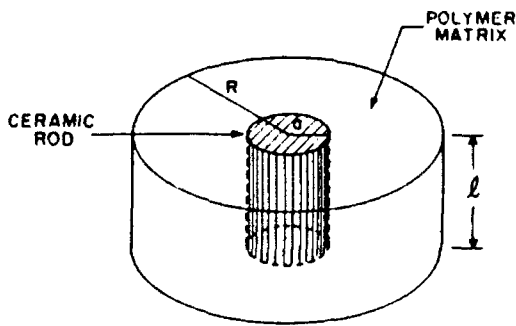


FIG. 1. A single ceramic rod composite of length l . The radius of the composite is R and a is the radius of the ceramic rod.

ceramic rods are poled in the axial direction (the z direction in our calculations), the stress transfer in the 1-3 structure only enhances the piezoelectric response of the ceramic rods in the z direction. Therefore, to a good approximation, we only need to derive the z component of the displacement field. Following the procedure described in Ref. 6, we use the ansatz $u(r,z) = (2z/l)u(r,l/2)$, for the z component of the displacement field; then, under a uniaxial stress T_3 , the static equilibrium condition for the polymer and ceramic phases can be written in the following form in a cylindrical coordinate system:

$$\frac{\mu^p l}{4} \left(\frac{\partial^2 u(r,l/2)}{\partial r^2} + \frac{1}{r} \frac{\partial u(r,l/2)}{\partial r} + \frac{1}{r^2} \frac{\partial^2 u(r,l/2)}{\partial \phi^2} \right) = \frac{2Y^p}{l} u(r,l/2) - T_3, \quad r > a, \quad (1a)$$

$$\frac{c_{44} l}{4} \left(\frac{\partial^2 v(r,l/2)}{\partial r^2} + \frac{1}{r} \frac{\partial v(r,l/2)}{\partial r} + \frac{1}{r^2} \frac{\partial^2 v(r,l/2)}{\partial \phi^2} \right) = \frac{2}{ls_{33}} v(r,l/2) - T_3, \quad r < a, \quad (1b)$$

where $u(r,l/2)$ and $v(r,l/2)$ are the z components of the displacement for the polymer and the ceramic, respectively, at the top surface of the composite. μ^p and Y^p denote the shear and Young's moduli of the polymer phase, and

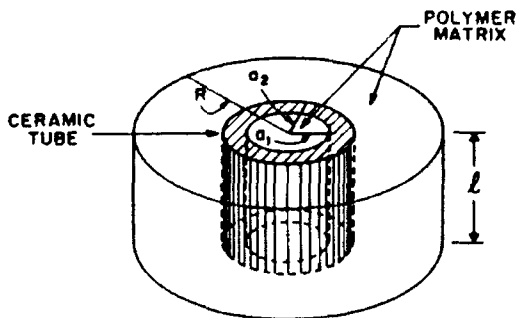


FIG. 2. A single ceramic tube composite of length l . The radius of the composite is R , while a_1 and a_2 are the inner and outer radii of the ceramic tube.

c_{44} and s_{33} are the shear elastic stiffness and the normal elastic compliance of the ceramic, respectively.

Considering the composite shown in Fig. 1, the solution must be independent of ϕ because of the symmetry, which means that the second derivative with respect to ϕ vanishes. By making the following substitution

$$\bar{u} = u(r,l/2) - (lT_3/2Y^p), \quad (2a)$$

$$\rho = r/\xi^p, \quad \xi^p = (l/2) \sqrt{\mu^p/2Y^p}, \quad (2b)$$

Eq. (1a) can be recast to the following zeroth-order Bessel equation of imaginary argument:

$$\rho^2 \frac{\partial^2 \bar{u}}{\partial \rho^2} + \rho \frac{\partial \bar{u}}{\partial \rho} - \rho^2 \bar{u} = 0. \quad (3)$$

Standard solutions exist for Eq. (3) so that the surface displacement of the polymer phase, $u(r,l/2)$, can be obtained using Eqs. (2a) and (2b),

$$u\left(r, \frac{l}{2}\right) = AK_0\left(\frac{r}{\xi^p}\right) + BI_0\left(\frac{r}{\xi^p}\right) + \frac{l}{2Y^p} T_3 \quad (r > a) \quad (4)$$

where $K_0(\rho)$ and $I_0(\rho)$ are the zeroth-order modified Bessel functions, and A and B are the constants of integration.

Similarly we can obtain the surface displacement profile for the ceramic rod by solving Eq. (1b) using the same technique,

$$v(r,l/2) = CI_0(r/\xi^c) + (l/2)s_{33}T_3 \quad (r < a), \quad (5)$$

where $\xi^c = l/2 \sqrt{s_{33}c_{44}/2}$. Note that in Eq. (5) we have used the boundary condition that $v(r,l/2)$ is finite at $r=0$, so that only one integration constant C remains.

In order to determine the integration constants in the solutions Eqs. (4) and (5), three boundary conditions are needed. The first one can be obtained from the nonslip interface condition at $r=a$, viz.

$$u(a,l/2) = v(a,l/2). \quad (6)$$

The second one is the free-boundary condition at $r=R$ for the polymer phase,

$$\left. \frac{\partial u(r,l/2)}{\partial r} \right|_{r=R} = 0 \quad (7)$$

[the derivative of $u(r,z)$ along the direction normal to the unit-cell boundary must always vanish in the composite structure due to symmetry]. For the single-rod composite in Fig. 1 we can use Newton's third law to derive the other condition needed to determine the constants as described

TABLE I. Elastic, piezoelectric, and dielectric constants of PZT5H^a and epoxy^b used in our calculations. ϵ_0 is the dielectric constant of vacuum.

PZT5H: $s_{11} = 0.0208$ (10^{-9} m ² /N), $c_{44} = 20.0$ (10^9 N/m ²), $\sigma^c = 0.31$, $d_{31} = 593$ (10^{-12} C/N), $d_{11} = -274$ (10^{-12} C/N), $\epsilon^c = 3400\epsilon_0$
Epoxy: $Y^p = 3.1$ (10^9 N/m ²), $\mu^p = 1.148$ (10^9 N/m ²), $\sigma = 0.35$, $\epsilon^p = 3.5\epsilon_0$

^aSee Ref. 7.

^bSee Ref. 8.

in Ref. 6, but for later convenience, we use the following equivalent but more general boundary condition:

$$\mu^p \frac{\partial u(r, l/2)}{\partial r} \Big|_{r=a} = c_{44} \frac{\partial v(r, l/2)}{\partial r} \Big|_{r=a} \quad (8)$$

Equation (8) states that the shear stress is a continuous function of r across the interface in the nonslip interface composite structures.

Now the three integration constants A , B , and C can be determined from Eqs. (6), (7), and (8); they are

$$A = \frac{-(l/2)I_1(\rho_R^p)I_1(\rho_a^c)(1/Y^p - s_{33})T_3}{\sqrt{(Y^p s_{33} \mu^p / c_{44})I_0(\rho_a^c)[I_1(\rho_R^p)K_1(\rho_a^c) - I_1(\rho_a^c)K_1(\rho_R^p)] + I_1(\rho_a^c)[I_1(\rho_R^p)K_0(\rho_a^c) + K_1(\rho_R^p)I_0(\rho_a^c)]}} \quad (9a)$$

$$B = \frac{(l/2)K_1(\rho_R^p)I_1(\rho_a^c)(1/Y^p - s_{33})T_3}{\sqrt{(Y^p s_{33} \mu^p / c_{44})I_0(\rho_a^c)[I_1(\rho_R^p)K_1(\rho_a^c) - I_1(\rho_a^c)K_1(\rho_R^p)] + I_1(\rho_a^c)[I_1(\rho_R^p)K_0(\rho_a^c) + K_1(\rho_R^p)I_0(\rho_a^c)]}} \quad (9b)$$

$$C = \frac{(l/2)\{I_1(\rho_R^p)K_1(\rho_a^c) - I_1(\rho_a^c)K_1(\rho_R^p)\}(1/Y^p - s_{33})T_3}{I_1(\rho_a^c)[I_1(\rho_R^p)K_1(\rho_a^c) - I_1(\rho_a^c)K_1(\rho_R^p)] + \sqrt{(c_{44}/Y^p s_{33} \mu^p)I_1(\rho_a^c)[I_1(\rho_R^p)K_0(\rho_a^c) + K_1(\rho_R^p)I_0(\rho_a^c)]}} \quad (9c)$$

where

$$\rho_a^p = a/\xi^p, \quad \rho_R^p = R/\xi^p, \quad \rho_a^c = a/\xi^c,$$

and $K_0(\rho)$, $I_0(\rho)$, $K_1(\rho)$, and $I_1(\rho)$ are the zeroth- and first-order modified Bessel functions.

Because of the coupling between the two components at the interface in the 1-3 structure, the total effective stress on the ceramic becomes larger but inhomogeneous. The magnitude of the effective total stress is the largest at the interface and becomes smaller away from the interface. The effective induced electric displacement in the ceramic now becomes

$$D(r) = d_{33} T_3^{\text{eff}} = \frac{d_{33} v(r, l/2)}{s_{33} l/2}, \quad r < a. \quad (10)$$

From Eq. (10) we can calculate the total bound charge Q produced at the top surface of the ceramic rod,

$$Q = 2\pi \int_0^a D(r) r dr = \gamma d_{33} T_3 \pi a^2, \quad (11)$$

where

$$\gamma = 1 + \frac{(l/a)I_1(\rho_a^c)[I_1(\rho_R^p)K_1(\rho_a^c) - I_1(\rho_a^c)K_1(\rho_R^p)](1/Y^p - s_{33})}{\sqrt{(2s_{33}/c_{44})I_0(\rho_a^c)[I_1(\rho_R^p)K_1(\rho_a^c) - I_1(\rho_a^c)K_1(\rho_R^p)] + \sqrt{(2/Y^p \mu^p)I_1(\rho_a^c)[I_1(\rho_R^p)K_0(\rho_a^c) + K_1(\rho_R^p)I_0(\rho_a^c)]}}} \quad (12)$$

is the stress amplification factor.

We can see that the amplification factor depends on the elastic properties of both phases, the ceramic content $V_c = a^2/R^2$, and more important, the aspect ratio a/l . In order to visualize this aspect ratio dependence, we have calculated the numerical values of Eq. (12) for a PZT5H-epoxy composite using the input data in Table I. (PZT5H is a trademark of Vernitron Corp. for its lanthanum-doped PZT product.) The results are shown in Fig. 3. Two important conclusions can be drawn from the results in Fig. 3 as follows.

(i) There is a saturation value for the enhancement effect for any given aspect ratio a/l . This is because the stress transfer effect is limited only to the portion near the ceramic-polymer interface; in other words, only the polymer portion near the interface actually contributes to the enhancement effect. This point will be elaborated below. This saturation value of γ can be derived from Eq. (12) by taking the limit $R \rightarrow \infty$,

$$\lim_{R \rightarrow \infty} \gamma = 1 + \frac{(l/a)K_1(\rho_a^p)I_1(\rho_a^c)(1/Y^p - s_{33})}{\sqrt{(2s_{33}/c_{44})I_0(\rho_a^c)K_1(\rho_a^p) + \sqrt{(2/Y^p \mu^p)I_1(\rho_a^c)K_0(\rho_a^p)}}} \quad (13)$$

This limiting value depends very strongly on the aspect ratio of the ceramic rod a/l , which may be visualized from the results shown in Fig. 3 at $V_c = 0$; it decreases rapidly with the increase of the ratio a/l . The inclusion of the aspect ratio is one of the novel features of the current model.

(ii) The γ value obtained from the current model is always smaller than the isostrain result but larger than the two-phase decoupling result ($\gamma = 1$, which can be obtained by taking the limit $a \rightarrow \infty$ for a finite l), depending on the aspect ratio a/l of the structure. In general, for a fixed ceramic content, thin and long rods should be used in order to get larger γ . The isostrain models actually give the upper limit for the enhancement factor, which can be derived from Eq. (12) for a finite R by taking the limit $l \rightarrow \infty$,

$$\lim_{l \rightarrow \infty} \gamma = \frac{1}{V_c + V_p Y^p s_{33}}, \quad (14)$$

where V_c and V_p are the volume fractions of the ceramic and polymer respectively. Equation (14) is just the isostrain result.⁹

In order to see how the stress transfer actually takes place, the generated additional stress T_{add} inside both the ceramic and the polymer phases for a single-rod composite

is calculated using the parameters from Table I. For clarity and simplicity, we assume $R \rightarrow \infty$ (corresponding to $V_c \rightarrow 0$); then the solutions for the z component of the displacement field inside the composite become

$$u(r, z) = \frac{z}{l/2} \left(AK_0(\rho^p) + \frac{l/2}{Y^p} T_3 \right), \quad r > a, \quad (15a)$$

$$v(r, z) = \frac{z}{l/2} \left(CI_0(\rho^c) + \frac{l}{2} s_{33} T_3 \right), \quad r < a, \quad (15b)$$

where

$$A = \frac{(l/2) I_1(\rho_a^c) (s_{33} - 1/Y^p) T_3}{\sqrt{(Y^p s_{33} \mu^p / c_{44}) I_0(\rho_a^c) K_1(\rho_a^c) + I_1(\rho_a^c) K_0(\rho_a^c)}}, \quad (16a)$$

$$C = \frac{(l/2) K_1(\rho_a^p) (1/Y^p - s_{33}) T_3}{I_0(\rho_a^c) K_1(\rho_a^c) + \sqrt{(c_{44} / Y^p s_{33} \mu^p) I_1(\rho_a^c) K_0(\rho_a^c)}}. \quad (16b)$$

In this case the generated additional stress T_{add} is

$$T_{\text{add}} = T_3^{\text{eff}} - T_3 = \begin{cases} \frac{I_1(\rho_a^c) (s_{33} Y^p - 1) T_3 K_0(\rho^p)}{\sqrt{(Y^p s_{33} \mu^p / c_{44}) I_0(\rho_a^c) K_1(\rho_a^c) + I_1(\rho_a^c) K_0(\rho_a^c)}}, & r > a, \\ \frac{K_1(\rho_a^p) (1/Y^p s_{33} - 1) T_3 I_0(\rho^c)}{I_0(\rho_a^c) K_1(\rho_a^c) + \sqrt{(c_{44} / Y^p s_{33} \mu^p) I_1(\rho_a^c) K_0(\rho_a^c)}}, & r < a. \end{cases} \quad (17a)$$

$$(17b)$$

T_{add} is plotted in Fig. 4 for a single-rod PZT5H-epoxy composite with $a=0.5$, $l=2.5$ and 5 , respectively. We can see that T_{add} has opposite signs in the ceramic ($r < 0.5$) and in the polymer ($r > 0.5$), and the magnitude is the largest at the interface. There is a substantial increase of the effective stress in the ceramic at the expense of the stress reduction in the polymer phase. Because of the difference between the elastic properties in the two phases, T_{add} subsides very fast away from the interface in the polymer but changes relatively slowly in the ceramic phase. Also, we note in Fig. 4 that T_{add} depends very strongly on

the ratio a/l . With the increase of l , more polymer will participate in the stress transfer process. Although the maximum stress magnitude at the interface $a=0.5$ becomes slightly smaller, the total force transferred to the ceramic rod, which is the product of the stress and the surface area of the participating polymer, becomes larger. We found that the inhomogeneity of the additional stress becomes stronger as the a/l ratio increases.

It is clear from the stress analysis that the most effective portion of the 1-3 structure is near the ceramic-polymer interface, especially for relatively large a/l ratio. Therefore, one of the fundamental guidelines for the structural design of 1-3 composite is to increase the ceramic-polymer interface area.

We now proceed to calculate the hydrostatic piezoelectric constant for the single-rod 1-3 composite shown in Fig. 1. The boundary condition for this problem should be constant stress on all surfaces of the composite. However, this boundary condition is not satisfied in the previous theoretical models which assumed isostrain boundary condition in the axial direction of the rods. Therefore, the effective hydrostatic piezoelectric constant of the 1-3 structure calculated from the previous models is often much larger than the experimental values.^{5,9} The simple parallel model and series model could not give the right result because the conditions of isostrain in the z direction and equal stress in the x and y directions are self-contradictory. When stresses are applied in the x and y directions, the induced displacement in the z direction will be quite different in the ceramic and polymer phases, due to the difference in elastic com-

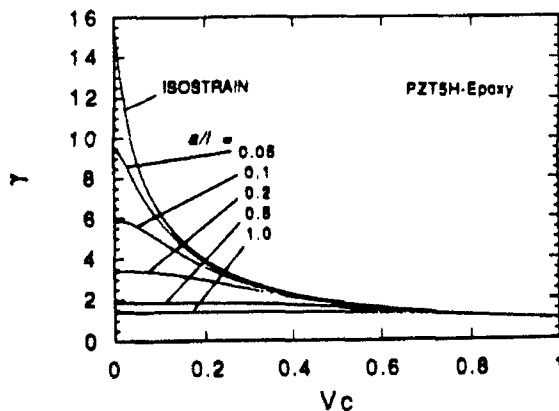


FIG. 3. Calculated dependence of the amplification factor γ on the ceramic content for a PZT5H-epoxy composite with the following aspect ratio: $a/l=0.05, 0.1, 0.2, 0.5$, and 1.0 . The uppermost line is the isostrain result.

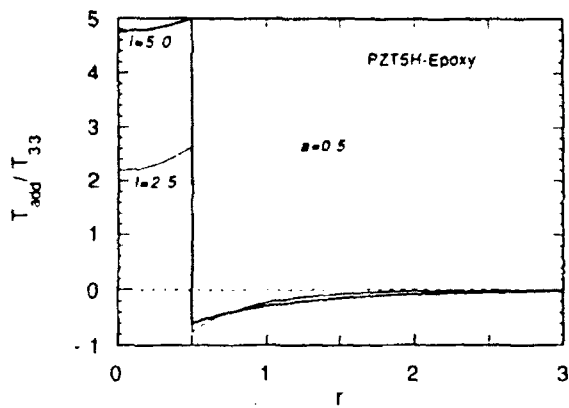


FIG. 4. Concentration of the generated additional stress T_{add} as a function of r for a single-rod PZT5H-epoxy 1-3 composite under a uniaxial stress T_3 . The radius of the ceramic rod is 0.5. The thick line is for $l=5$ and the thin line for $l=2.5$. The maximum value of the additional stress appears at the interface $r=0.5$, and the signs of the stresses in the two phases are opposite.

pliance. Although the series model may be used in the x and y direction, the equal strain model must not be used in the z direction unless infinitely stiff plates are placed on the two surfaces of the composite. In order to adequately calculate the hydrostatic piezoelectric constant for the 1-3 composite, one must consider all three dimensions simultaneously and the solution should satisfy equal stress boundary conditions in all three dimensions.

Before we calculate the effective hydrostatic piezoelectric constant of the composite structure, let us discuss briefly the physics involved in the 1-3 structure. Equation (1) may be rewritten in the following form:

$$\frac{2}{l} u \left(r, \frac{l}{2} \right) = s_{33}^p \left[T_3 + \frac{\mu^p l}{4} \left(\frac{\partial^2 u(r, l/2)}{\partial r^2} + \frac{1}{r} \frac{\partial u(r, l/2)}{\partial r} + \frac{1}{r^2} \frac{\partial^2 u(r, l/2)}{\partial \phi^2} \right) \right], \quad (18)$$

where $s_{33}^p = 1/Y^p$ is the normal elastic compliance of the polymer. Equation (18) tells us that, in the composite, the effective T_3^{eff} [in the square bracket of Eq. (18)] is inhomogeneous due to the additional stress generated by the nonslip ceramic-polymer interface, although the applied stress T_3 is homogeneous. While in the other two dimen-

sions, there is no interface enhancement effect, the stress will still be homogeneous, but the stresses applied in the directions perpendicular to the z direction can generate additional stress in the z direction due to the Poisson's ratio effect and the difference of elastic compliance in the two phases. When normal stresses are applied in all three dimensions, the local strain-stress relation in the z direction inside the polymer may be written as

$$\frac{2}{l} u \left(r, \frac{l}{2} \right) = s_{33}^p \left[T_3 + \frac{\mu^p l}{4} \left(\frac{\partial^2 u(r, l/2)}{\partial r^2} + \frac{1}{r} \frac{\partial u(r, l/2)}{\partial r} + \frac{1}{r^2} \frac{\partial^2 u(r, l/2)}{\partial \phi^2} \right) \right] + s_{31}^p T_1 + s_{31}^p T_2. \quad (19)$$

For the case of hydrostatic pressure, $T_1 = T_2 = T_3 = -P$, Eq. (19) becomes

$$\frac{\mu^p l}{4} \left(\frac{\partial^2 u(r, l/2)}{\partial r^2} + \frac{1}{r} \frac{\partial u(r, l/2)}{\partial r} + \frac{1}{r^2} \frac{\partial^2 u(r, l/2)}{\partial \phi^2} \right) = \frac{2Y^p}{l} u \left(r, \frac{l}{2} \right) + (1-2\sigma)P, \quad (20)$$

where $\sigma = s_{31}^p/s_{33}^p$ is the Poisson's ratio for the polymer. Equation (20) is identical to Eq. (1a) if we replace T_3 with $-(1-2\sigma)P$. Similarly one can reach the same conclusion for the ceramic phase, except in this case we must replace T_3 by $-(1-2\sigma^c)P$, with $\sigma^c = s_{31}^c/s_{33}^c$.

Now the electric displacement in the ceramic under a hydrostatic pressure can be written as

$$D(r) = d_{33} \left[T_3 + \frac{c_{44} l}{4} \left(\frac{\partial^2 v(r, l/2)}{\partial r^2} + \frac{1}{r} \frac{\partial v(r, l/2)}{\partial r} + \frac{1}{r^2} \frac{\partial^2 v(r, l/2)}{\partial \phi^2} \right) \right] + d_{31} T_1 + d_{32} T_2 = d_{33} \left(\frac{2v(r, l/2)}{l s_{33}^c} - 2\sigma^c P \right) - 2d_{31} P. \quad (21)$$

Equation (21) includes both the Poisson's ratio effect and the interface enhancement.

From Eq. (11) the total charge Q produced by the hydrostatic pressure P can be obtained by integrating Eq. (21) over the end surface of the ceramic rod,

$$Q = -\pi a^2 (\gamma_h d_{33} + 2d_{31}) P, \quad (22)$$

where

$$\gamma_h = 1 + \frac{(l/a) I_1(\rho_a^c) [I_1(\rho_R^p) K_1(\rho_a^p) - I_1(\rho_a^p) K_1(\rho_R^p)] [(1-2\sigma)/Y^p - (1-2\sigma^c) s_{33}]}{\sqrt{(2s_{33}/c_{44}) I_0(\rho_a^c) [I_1(\rho_R^p) K_1(\rho_a^p) - I_1(\rho_a^p) K_1(\rho_R^p)]} + \sqrt{(2/Y^p \mu^p) I_1(\rho_a^c) [I_1(\rho_R^p) K_0(\rho_a^p) + K_1(\rho_R^p) I_0(\rho_a^p)]}} \quad (23)$$

is the amplification factor in the hydrostatic situation. Compared to Eq. (12), the only difference is the inclusion of the Poisson's ratio effect, i.e., the two factors $(1-2\sigma)$ and $(1-2\sigma^c)$.

From Eq. (22) the effective hydrostatic piezoelectric

constant \bar{d}_h of the composite is therefore given by

$$\bar{d}_h = (\gamma_h d_{33} + 2d_{31}) (a^2/R^3) = V_c (\gamma_h d_{33} + 2d_{31}), \quad (24)$$

where V_c is the volume fraction of the ceramic. Equation (24) is plotted in Fig. 5 for several different aspect ratios

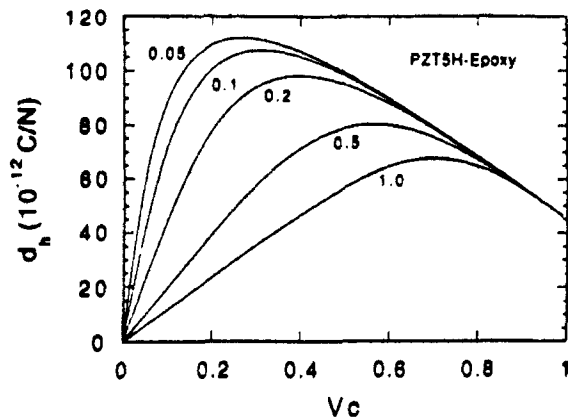


FIG. 5. The hydrostatic piezoelectric constant \bar{d}_h as a function of the ceramic content at a/l ratios of 0.05, 0.1, 0.2, 0.5, and 1.0 for a single-rod PZT5H-epoxy 1-3 composite.

for a PZT5H-epoxy composite using the input data from Table I. \bar{d}_h shows a peak value for each value of a/l ; this peak value appears at about 25% for $a/l=0.05$ and shifts to higher ceramic content with the increase of a/l . The peak value increases with the decrease of the ratio a/l ; however, there is a saturation of the aspect ratio effect as one can see from Fig. 5. We found that the curve for $a/l=0.05$ is already very close to the saturated value; very little improvement is obtained when the ratio is further decreased to $a/l=0.02$. The curves for $a/l=0.02$ and 0.01 are practically the same.

The 1-3 structure also increases the effective piezoelectric charge constant g_h because the effective dielectric constant of the composite is reduced. For hydrostatic applications the conventional criterion for the 1-3 composites is the hydrostatic figure of merit which is defined as $g_h \bar{d}_h$. For the 1-3 structure, it can be written as follows:

$$\bar{g}_h \bar{d}_h = \frac{\bar{d}_h^2}{(\epsilon^c - \epsilon^p)V_c + \epsilon^p} \quad (25)$$

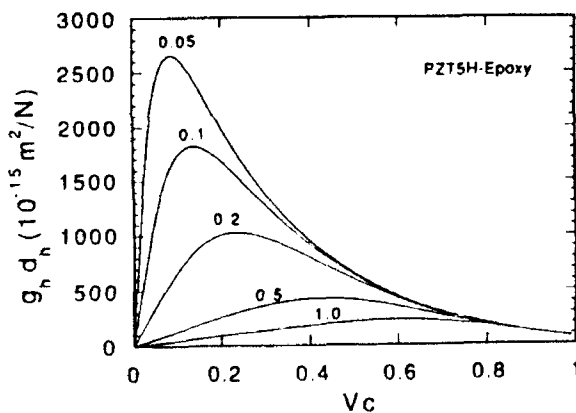


FIG. 6. The figure of merit, $\bar{g}_h \bar{d}_h$, as a function of the ceramic content with the a/l ratios of 0.05, 0.1, 0.2, 0.5, and 1.0, respectively, for a single-rod PZT5H-epoxy 1-3 composite.

Figure 6 is the plot of Eq. (25) as a function of the ceramic content at four different aspect ratios for the PZT5H-epoxy composite using the input data from Table I. One can see that the figure of merit also strongly depends on the ratio a/l . In the commonly used range of the aspect ratio, the hydrostatic figure of merit can be well over $2000 \times 10^{-15} \text{ m}^2/\text{N}$ for the optimized structure, which is much larger than the conventional piezoelectric ceramics.

III. SOLUTIONS FOR A SINGLE CERAMIC TUBE COMPOSITE

The stress distribution in Fig. 4 tells us that the most useful parts for the stress transfer are those near the ceramic-polymer interface, which suggests that the shape of the ceramic component should be designed to have larger interface area with the polymer. An immediate design possibility would be to replace the ceramic rods with tubes, since for thin wall tubes the interface area can be substantially increased as compared to the solid rods for the same ceramic content. Clearly, from the principle of stress transfer, the structure will be more effective if the interior of the tube is filled with polymer assuming no surface cracking. The unit cell for this case is plotted in Fig. 2. In what follows we only give the results for the filled interior tube composite. One can easily derive the solutions for the case of empty interior tube composite following the same procedure.

As shown in the previous section, the hydrostatic case may be treated the same way as the uniaxial case for the 1-3 composite systems. Therefore, we only need to consider the situation of the composite under a uniaxial stress T_3 . For the tube composite the unit cell contains three different regions: $r < a_1$; $a_1 < r < a_2$; and $a_2 < r < R$ as shown in Fig. 2. The surface displacement profiles of the composite in the three regions are, respectively, given by

$$u\left(r, \frac{l}{2}\right) = \begin{cases} A_1 I_0\left(\frac{r}{\xi^p}\right) + \frac{l T_3}{2 Y^p}, & r < a_1, \\ B_1 K_0\left(\frac{r}{\xi^p}\right) + B_2 I_0\left(\frac{r}{\xi^p}\right) + \frac{l T_3}{2 Y^p}, & a_1 < r < R, \end{cases} \quad (26)$$

$$v\left(r, \frac{l}{2}\right) = C_1 K_0\left(\frac{r}{\xi^c}\right) + C_2 I_0\left(\frac{r}{\xi^c}\right) + \frac{l}{2} s_{33} T_3, \quad a_1 < r < a_2. \quad (27)$$

The five integration constants in Eqs. (26) and (27) can be obtained using the same boundary conditions as given in Eqs. (6)-(8) at $r=a_1$, a_2 , and R , respectively. Because the expressions for these constants are lengthy, we define the following quantities:

$$\begin{aligned}
I_{01} &= I_0(a_1/\xi^p), & I_{02} &= I_0(a_2/\xi^p), & I_{11} &= I_1(a_1/\xi^p), \\
K_{01} &= K_0(a_1/\xi^c), & I_{0\bar{1}} &= I_0(a_1/\xi^c), & I_{0\bar{2}} &= I_0(a_2/\xi^c), \\
I_{1\bar{1}} &= I_1(a_1/\xi^c), & K_{0\bar{2}} &= K_0(a_2/\xi^c), & I_{12} &= I_1(a_2/\xi^p), \\
I_{1\bar{2}} &= I_1(a_2/\xi^c), & K_{02} &= K_0(a_2/\xi^p), & K_{12} &= K_1(a_2/\xi^p)
\end{aligned}$$

$$K_{1\bar{1}} = K_1(a_1/\xi^c), \quad K_{1\bar{2}} = K_1(a_2/\xi^c),$$

$$I_{1R} = I_1(R/\xi^p), \quad K_{1R} = K_1(R/\xi^p).$$

In terms of these abbreviations the integration constants in Eqs. (25) and (26) can be written as

$$A_1 = \beta [I_{1\bar{1}}(K_{0\bar{1}} - K_{0\bar{2}} - \lambda K_{1\bar{2}}) + K_{1\bar{1}}(I_{0\bar{1}} + I_{0\bar{2}} - \lambda I_{1\bar{2}})] T_3, \quad (28)$$

$$B_1 = \frac{\beta I_{1R} [R^E I_{01} (I_{1\bar{2}} K_{1\bar{1}} - I_{1\bar{1}} K_{1\bar{2}}) + I_{11} I_{1\bar{2}} (K_{0\bar{1}} - I_{0\bar{2}}) + I_{11} K_{1\bar{2}} (I_{0\bar{1}} + I_{0\bar{2}})] T_3}{I_{12} K_{1R} - I_{1R} K_{12}}, \quad (29)$$

$$B_2 = \frac{\beta K_{1R} [R^E I_{01} (I_{1\bar{2}} K_{1\bar{1}} - I_{1\bar{1}} K_{1\bar{2}}) + I_{11} I_{1\bar{2}} (K_{0\bar{1}} - I_{0\bar{2}}) + I_{11} K_{1\bar{2}} (I_{0\bar{1}} + I_{0\bar{2}})] T_3}{I_{12} K_{1R} - I_{1R} K_{12}}, \quad (30)$$

$$C_1 = \beta [R^E I_{01} I_{1\bar{1}} - I_{11} (I_{0\bar{1}} + I_{0\bar{2}} + \lambda I_{1\bar{2}})] T_3, \quad (31)$$

$$C_2 = \beta [R^E I_{01} K_{1\bar{1}} + I_{11} (K_{0\bar{1}} - K_{0\bar{2}} - \lambda K_{1\bar{2}})] T_3, \quad (32)$$

where

$$R^E = \sqrt{c_{44}/s_{33}\mu^p Y^p}, \quad \lambda = R^E (I_{1R} K_{02} + I_{02} K_{1R}) / (I_{12} K_{1R} - I_{1R} K_{12}),$$

and

$$\beta = \frac{(1/Y^p - s_{33})/2}{R^E I_{01} (I_{1\bar{1}} K_{0\bar{2}} + \lambda I_{1\bar{1}} K_{1\bar{2}} - \lambda I_{1\bar{2}} K_{1\bar{1}} + K_{1\bar{1}} I_{0\bar{2}}) - I_{11} (I_{0\bar{1}} K_{0\bar{2}} + \lambda I_{0\bar{1}} K_{1\bar{2}} + \lambda I_{1\bar{2}} K_{0\bar{1}} - I_{0\bar{2}} K_{0\bar{1}})}.$$

Similar to the previous section, one can find the total charge Q produced at the top surface of the ceramic tube under a uniaxial stress T_3 ,

$$Q = 2\pi \int_{a_1}^{a_2} \frac{2d_{33}}{s_{33}} v \left(r, \frac{l}{2} \right) r dr = \gamma d_{33} T_3 \pi (a_2^2 - a_1^2), \quad (33)$$

where

$$\begin{aligned}
\gamma &= 1 + \frac{\sqrt{2c_{44}/s_{33}}}{T_3 (a_2^2 - a_1^2)} \{ C_1 (a_1 K_{1\bar{1}} - a_2 K_{1\bar{2}}) \\
&\quad + C_2 (a_2 I_{1\bar{2}} - a_1 I_{1\bar{1}}) \} \quad (34)
\end{aligned}$$

is the stress amplification factor for the tube composite under uniaxial stress. One can verify that Eq. (34) recovers the result of Eq. (12) in the limit of $a_1 \rightarrow 0$.

In Fig. 7 we have plotted Eq. (34) for a single-tube composite of $l=5$ and $R=5$. The ceramic fractions are 0.01, 0.02, 0.05, 0.1, 0.2, and 0.5, respectively, as labeled in the figure. One can see that for each specified ceramic volume percentage the γ value increases with the increase of the inner radius of the tube a_1 at the beginning, then decreases slightly after reaching a peak value. For the 1% ceramic composite, the γ value can be increased by as much as a factor of 2 compared to the ceramic rod composite ($a_1=0$, and for the corresponding 1% ceramic single-rod composite the a/l ratio is 0.1). The slight decrease of γ for large a_1 is caused by the gradual disappearance of the outer interface in the structure, as one can see

that the ceramic tube becomes the outer shell for the structure when a_1 is sufficiently large, i.e., $a_2=R$.

Due to the increase of the interface area in the tube ceramic configuration, the effective volume of the polymer that participates in the stress transfer becomes larger. As a result, more charges are produced for the same ceramic content compared with the solid rod composite. In other words, the ceramic tubes are more effective for stress transfer than the solid ceramic rods in the 1-3 composite structure. In principle, other ceramic geometries can also be analyzed in the same manner. However, the displacement field will also depend on the angular variable ϕ for noncylindrical symmetries, which may defy an analytic solution.

IV. SUMMARY AND CONCLUSIONS

A theoretical study has been carried out for the 1-3-type composites based on the model developed in Ref. 6. As examples, a single-rod and single-tube composite have been treated for cylindrical symmetry. Analytic solutions are obtained for the inhomogeneous surface displacements in the z direction under both uniaxial and hydrostatic stress. From these inhomogeneous displacement solutions, the effective piezoelectric constants of 1-3 composites can be calculated.

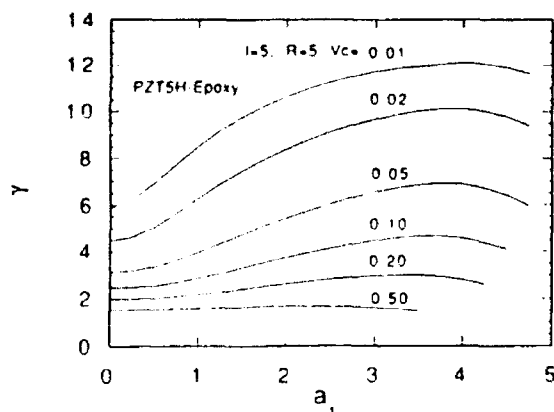


FIG. 7. The change of the amplification factor γ for a single-tube composite with the inner radius of the ceramic tube a_1 for the following volume fractions of ceramic: 0.01, 0.02, 0.05, 0.1, 0.2, and 0.5.

The stress transfer in the 1-3 composites is accomplished through shear coupling at the interface between the two components. Because of the difference in elastic compliance, the two phases cannot have isostrain under uniaxial or hydrostatic stress without surface capping. The effectiveness of the stress transfer can be characterized by a stress amplification factor γ defined in Eqs. (12), (23), and (34). This stress amplification factor is shown to depend on the elastic properties of both phases, the ceramic content, and, more important, the aspect ratio of the ceramic rods. It is shown that the stress transfer effect practically vanishes if the ratio $a/l > 1$. We have also demonstrated that the hydrostatic stress case can be treated in the same way as the uniaxial stress. However, because of the Poisson's ratio effect, the stresses applied in the directions perpendicular to the axial direction of the rod reduces the enhancement effect in the axial direction. Hence, under hydrostatic pressure the amplification factor γ_h is practically reduced by a factor of $(1-2\sigma)$ due to the Poisson's ratio effect, where σ is the Poisson's ratio.

Through the stress analyses, we have shown clearly that the most effective portion of the polymer for the stress transfer is in the vicinity of the ceramic-polymer interface. Therefore, the optimum design for the 1-3 composite structure should contain maximum interface area. If the ceramic volume content and the thickness of the 1-3 structure are fixed, the composite made of ceramic tubes is more effective than the composite made of solid rods due to larger interface area.

In a real 1-3 composite structure the outside boundary of the unit cell is not circular, and the cross section of the ceramic rods may have square or other geometries, for which one must solve each case according to the specified boundary conditions. In general, it may not be possible to obtain closed form expressions, one may have to resort to numerical methods. However, at very low ceramic content, i.e., if the rods are sufficiently far from each other, the single-rod solution obtained here is a very good first-order

approximation. Looking at the stress analyses in Fig. 4, we note that the polymer beyond $r=2.5$ actually contributed very little in the stress transfer. This rod distance corresponds to a ceramic volume percentage of about 4%. Therefore, the solutions derived here should be accurate for any rod arrangement if the ceramic content is less than 4%. We have shown that the calculated piezoelectric constant is comparable to the experimental result even for up to 20% ceramic.¹⁰

Through this theoretical study we have gained substantial insight into the fundamental principles of the 1-3 piezoelectric composite structure, including the mechanism of stress transfer and the influence of the aspect ratio. Several design principles for the 1-3 structure can therefore be stated based on the current study as follows.

(i) The ratio a/l should be relatively small. However, one must note that the enhancement of the stress transfer through reducing the a/l ratio has an upper limit. In the PZT5H-epoxy system (see Fig. 3), if $a/l=0.02$, the γ value essentially reaches the upper limit. Thus, there is no benefit in making the ratio a/l less than 0.02 for this system since the decrease of a/l ratio of the ceramic rods often increases the difficulties in manufacturing 1-3 composites. Using our theoretical results, one can select the design parameters to optimize the performance of 1-3 composites for a specific purpose and at the same time minimize the cost of manufacturing.

(ii) The interface area between the two phases should be maximized so that the effective region of the polymer participating in the stress transfer is maximized.

(iii) From Eq. (14) one may conclude that the passive phase should be chosen to have the smallest possible Young's modulus (depending on the requirement of mechanical strength for the composite) in order to obtain a large γ . In addition, a larger ratio of the shear modulus versus Young's modulus for the passive phase is preferred, which can reduce the self loading of the polymer phase and increase the stress transferred to the ceramic phase. This might be achieved through a surface capping technique.

ACKNOWLEDGMENT

We would like to thank Dr. W. A. Smith for stimulating discussions.

¹R. E. Newnham, D. P. Skinner, and L. E. Cross, *Mater. Res. Bull.* 13, 525 (1978).

²D. P. Skinner, R. E. Newnham, and L. E. Cross, *Mater. Res. Bull.* 13, 599 (1978).

³W. A. Smith, A. Shaulov, and B. A. Auld, in *Proceedings of the 1985 IEEE Ultrasonics Symposium*, pp. 642-647.

⁴H. L. W. Chan and J. Unsworth, *IEEE Trans. Ultrasonics, Ferroelectrics and Frequency Control* UFFC-36, 434 (1989).

⁵K. A. Klicker, Ph.D. thesis, The Pennsylvania State University, University Park, PA, 1980.

⁶W. Cao, Q. Zhang, and L. E. Cross, *IEEE Trans. Ultrasonics, Ferroelectrics and Frequency Control* (to be published).

⁷Guide to Modern Piezoelectric Ceramic, from Morgan Matroc, Inc., Vernitron Division.

⁸C. G. Oakley, Ph.D. thesis, The Pennsylvania State University, 1991.

⁹M. J. Haun and R. E. Newnham, *Ferroelectrics*, 68, 123 (1986).

¹⁰Q. Zhang, W. Cao, H. Wang, and L. E. Cross, *J. Appl. Phys.* (to be published).

APPENDIX 4

STRAIN PROFILE AND PIEZOELECTRIC PERFORMANCE OF PIEZOCOMPOSITES WITH 2-2 AND 1-3 CONNECTIVITIES

Q. M. Zhang, Wnewu Cao, H. Wang, and L. E. Cross
Materials Research Laboratory, The Pennsylvania State University
University Park, PA 16802

Abstract: The piezoelectric performance of 1-3 type composite depends critically on the stress transfer between the two constituents phases. This paper presents the results of our recent investigation on the elastic and piezoelectric behaviors of composites with 2-2 and 1-3 connectivities. By taking into account the nonuniform strain profiles in the constituent phases, the theoretical model presented can quantitatively predict the performance of these composites. Theoretical predictions agree quantitatively with the experimental results.

Introduction

The quantitative study of the performance of piezoceramic-polymer composites is an interesting and challenging problem. In the past, a great deal of studies have been devoted to this subject.¹⁻³ Nevertheless, most of these studies are based on the effective medium theory, where the material properties in each constituent phase are assumed to be uniform, and the effective material parameters of a composite are calculated using either the parallel model (Voigt averaging) or series model (Reuss averaging). Although these studies provided general guidelines in predicting the composite properties, the quantitative predictions of the effective material parameters deviate from the experimental observations in most cases.

In this paper, we will present the results of our recent study on piezoceramic-polymer composites with 2-2 and 1-3 type connectivity.⁴⁻⁶ Since the most important factor of a composite structure is the stress transfer between the two constituent phases, the key to establish a working model for the composites is to understand how this stress transfer is realized. Illustrated in figure 1 is a 2-2 composite structure in which the ceramic plates and polymer are arranged parallel with each other. When subjected to a uniaxial stress, the composite will deform as illustrated by the dashed lines in figure 1(b). For comparison, we have also plotted in the same figure the deformation profile assuming no elastic coupling between the two constituent phases. The effectiveness of the stress transfer between the two phases depends on how much the strain in the polymer phase differs in the two situations [the area between the dash-dotted line and the dashed line in figure 1(b)]. This is determined by the elastic properties of the constituent phases and geometric factors of the composite. Clearly, the stress transfer in the composite is through the shear force and the strain in both phases is not uniform. When the strain is uniform in the composite, there is a maximum stress transfer between the two phases. This is the base for the isostrain model. However, to achieve that situation,

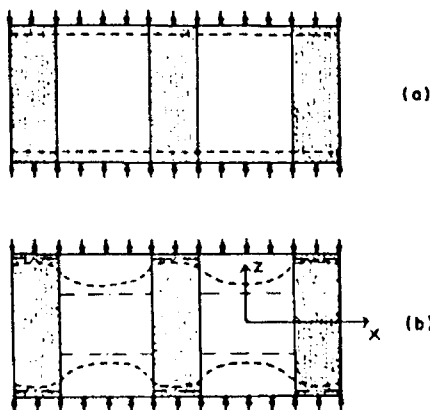


Figure 1: Schematic drawing of the 2-2 composite: (a) strain profile (dashed line) of the composite from the isostrain model when subjected to a uniaxial stress; (b) real strain profile (dashed line).

the shear modulus of the polymer phase needs to be infinity, which is not practical. This explains why the theoretical calculations based on the isostrain model always overestimate the piezoelectric response of composites. Shown in figure 2 is the strain profile for a 1-3 composite manufactured by Fiber Materials, Inc. The strain profile was measured by the double beam laser interferometer. Clearly, the strain in the polymer phase is much smaller than that expected from the isostrain model. The major advance of our model is to take into account this nonuniformity of the strain profile in the constituent phases explicitly. Therefore, this model can make quantitative predictions on the dependence of the effective material properties of a composite on the properties of its constituent phases and the sample geometric factors.

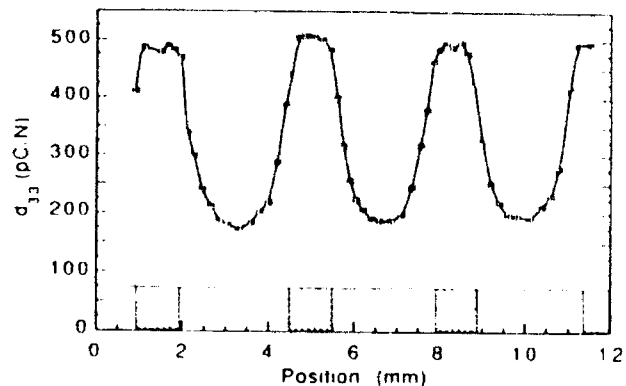


Figure 2: Strain profile for a 1-3 composite measured by the double beam laser interferometer. Hatched regions are PZT rods

The strain profile in 2-2 composites

The cross section of a 2-2 lamellar ceramic-polymer composite is shown in figure 3, where a and d are the dimensions of the ceramic plate and the polymer respectively in the x -direction, and L is the thickness of the composite in the z -direction. The dimension of the composite in the y -direction is much larger than L , a and d .

Under a uniaxial stress T_3 , both the polymer and the ceramic are either stretched or compressed depending on the sign of T_3 . From symmetry consideration, the $z=0$ plane (mirror plane) does not move at all in the z -direction. In the near static case, one can assume the strain to be uniform in the z -direction for any given x . Taking a segment as shown in figure 3 with unit length in the y -direction ($h=1$), the total shear force in the z -direction is

$$f_s = (L/4) \int_0^L \mu u_{xx}(x, L/2) dx$$

where $u(x, L/2)$ is the displacement profile at the top surface of the polymer, μ is the shear modulus of the polymer. In the x -direction the composite can move freely and the stress component in this direction is therefore zero. In the y -direction, the polymer is bounded by the ceramic plates and the total stress in this direction is lumped into T_2 since we are not interested in the details of this stress component. From these conditions, one can write down the constitutive relations for this elastic body

$$\frac{2u(x, L/2)}{L} = s_{33} \left(\frac{L}{4} \int_0^L \mu u_{xx}(x, L/2) dx \right) + T_3 + s_{32} T_2 \quad (1a)$$

$$S_2 = s_{22} T_2 + s_{12} \left(\frac{\mu L}{4} \int_0^L u_{xx}(x, L/2) dx \right) + T_3 \quad (1b)$$

where S_2 is the y -component of the strain in the polymer phase, s_{ij} is the elastic compliance. For the polymer, one has the relations $s_{22} = s_{33}$ and $s_{32}/s_{33} = -\sigma$, where σ is the Poisson's ratio. For a 2-2

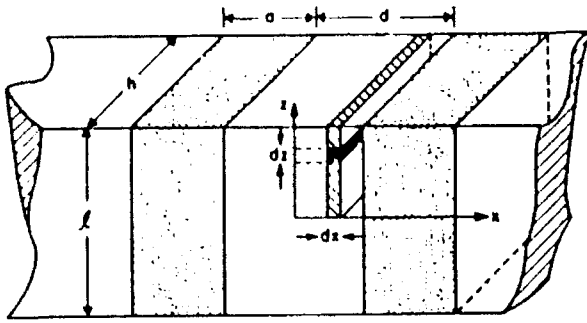


Figure 3: A section of 2-2 composite for our analysis.

composite with its y-dimension much larger than L, a and d, S_2 is practically a constant and is independent of x. That is, the strain in this direction can be modelled by the isostrain approximation. Combining eqs (1a) and (1b) to eliminate T_2 yields

$$\frac{2u(x, L/2)}{L} = s_{33}(1-\sigma^2) \frac{1}{4} \mu u_{xx}(x, L/2) + s_{33}(1-\sigma^2) T_3 - \sigma S_2 \quad (2)$$

If one neglects the stress effect in the y-direction, eq. (1) will be reduced to

$$\frac{2u(x, L/2)}{L} = s_{33} \frac{L}{4} \mu u_{xx}(x, L/2) + s_{33} T_3 \quad (3)$$

Hence, the effect of the y-direction stress on the strain in the z-direction is to modify the elastic compliance s_{33} to $s_{33}(1-\sigma^2)$ and to add an additional constant term (Poisson's ratio effect) in the equation. It does not affect the functional form of the equation. Considering the fact that both T_3 and S_2 are constants, we can make variable substitution: $v=u+(L/2)(\sigma S_2 - s_{33}(1-\sigma^2) T_3)$ and equation (2) becomes

$$\frac{2v(x, L/2)}{L} = s_{33}(1-\sigma^2) \frac{L}{4} \mu v_{xx}(x, L/2) \quad (4)$$

Therefore, the strain profile in the polymer phase between the two neighboring ceramic plates is

$$\frac{2u}{L} = A \cosh\left(2 \frac{x}{L} \sqrt{2Y/(\mu(1-\sigma^2))}\right) + \frac{T_3}{Y} - \sigma S_2 \quad (5)$$

where A is the integration constant, $Y=1/s_{33}$ is the Young's modulus of the polymer phase. $x=0$ is at the center of the polymer filling. A can be determined from the boundary condition: $A =$

$(2u_0/L - T_3/Y + \sigma S_2) / \cosh\left(\frac{d}{L} \sqrt{2Y/(\mu(1-\sigma^2))}\right)$, where $2u_0/L$ is the strain in the polymer-ceramic interface. For the situation when there is only one ceramic plate in the composite, the longitudinal strain of the polymer phase is

$$2u/L = B \exp\left(-\frac{(x-a/2)d}{L} \sqrt{2Y/(\mu(1-\sigma^2))}\right) + \frac{T_3}{Y} - \sigma S_2 \quad (x > a/2)$$

and

$$2u/L = B \exp\left(\frac{(x-a/2)d}{L} \sqrt{2Y/(\mu(1-\sigma^2))}\right) + \frac{T_3}{Y} - \sigma S_2 \quad (x < -a/2)$$

where $x=0$ is set at the center of the ceramic plate.

To compare with the theory, several 2-2 composites were made using PZT-5A plates embedded in spurs epoxy matrix. The longitudinal strain $S_3=2u/L$ of the sample was mapped out along a path parallel to the x-axis (refer to figure 1) using the double beam laser interferometer. Presented in figure 4 is the profile taken from one of these scans. The solid line in the figure is the fitting using eq. (5) for the polymer regions between the PZT plates and eq. (6) at the two edges of the sample. Clearly, the theoretical curve describes the data quite well. From fitting the data, one can obtain the value of $Y/(\mu(1-\sigma^2))=3.35$. For an isotropic medium, we have the relationship $Y/\mu=2(1-\sigma)$. Therefore, from the value of $Y/(\mu(1-\sigma^2))=3.35$, we can derive $\sigma=0.4$, which is a reasonable

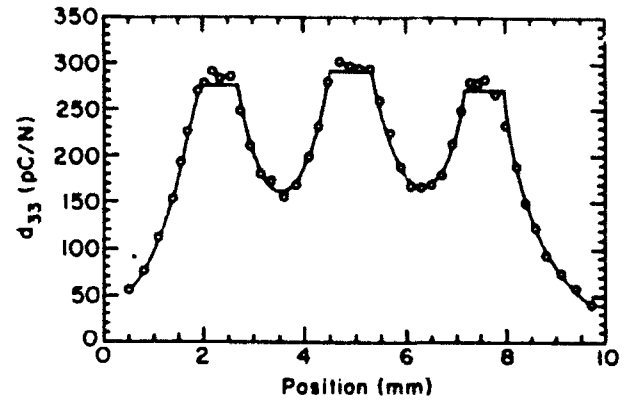


Figure 4: Comparison between the experimentally measured strain profile (dots in the figure) of a 2-2 composite and the theoretical curves (solid lines).

value for the spurs epoxy used.

Single rod 1-3 composite

Although the basic stress transfer mechanism between the two constituent phases in a 1-3 type composite is similar to that in the 2-2 type, the problem of solving the strain profile in a regular 1-3 composite is more involved and may be calculated numerically. Here we will only treat one special case, a single rod 1-3 composite subjected to a hydrostatic pressure, to show quantitatively how various parameters affect the performance of a 1-3 composite. The single rod composite is schematically drawn in figure 5, where a cylindrical coordinate system is used. This configuration is a reasonable approximation to the composite with triangularly arranged ceramic rods (for which the unit cell has hexagonal symmetry) and at low ceramic content, the results here could even be used for composites with other rod arrangements.⁶

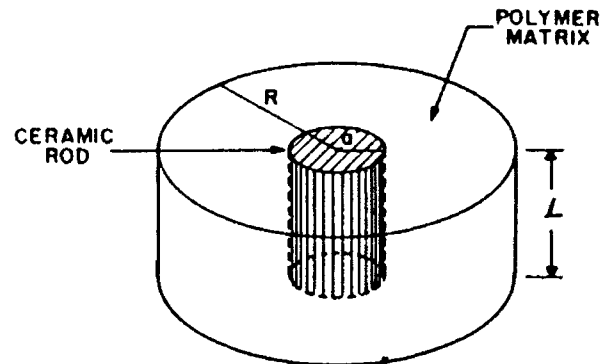


Figure 5: Schematic drawing of a single rod 1-3 composite.

Similar to the 2-2 composite situation, the force equilibrium condition for the polymer phase can be written in the following form⁶

$$\frac{\mu L}{4} (u_{rr}(r, L/2) + \frac{u_r(r, L/2)}{r}) - (1-2\sigma) p = \frac{2Y}{L} u(r, L/2) \quad (7)$$

where the meaning of each quantity is similar to that in the preceding section and p is the hydrostatic pressure. One can write down similar equation for the strain profile in the ceramic rod. The strain profile for the polymer phase is therefore given by

$$2u/L = A K_0(r/\xi) + B I_0(r/\xi) - (1-2\sigma) p/Y \quad (8)$$

where $K_0(p)$ and $I_0(p)$ are zeroth order modified Bessel functions. A and B can be determined from the boundary conditions. From the

strain profile, one can calculate the stress transfer between the two constituent phases and hence the effective piezoelectric hydrostatic strain constant d_h :

$$d_h = V_c (\gamma_h d_{33}^c + 2 d_{31}^c) \quad (9)$$

$$\gamma_h = 1 + \frac{\frac{L}{a} I_1(\rho_R)^c [I_1(\rho_R) K_1(\rho_R) - I_1(\rho_a) K_1(\rho_R)] [(1-2\sigma)/Y - (1-2\sigma^c) s_{33}]}{\sqrt{\frac{2s_{33}}{c_{44}} I_0(\rho_a)^c [I_1(\rho_R) K_1(\rho_a) - I_1(\rho_a) K_1(\rho_R)]} + \sqrt{\frac{2}{Y\mu} I_1(\rho_a)^c [I_1(\rho_R) K_0(\rho_a) + I_0(\rho_a) K_1(\rho_R)]}} \quad (10)$$

where s_{33} and c_{44} are the elastic compliance and the shear constant of the ceramic, σ^c is the Poisson's ratio of the ceramic,

$$\rho_r = (2r/L) \sqrt{\frac{2Y}{\mu}} \quad \text{and} \quad \rho_r^c = (2r/L) \sqrt{\frac{2}{s_{33}c_{44}}} \quad \text{One can see that}$$

the stress amplification factor depends on the elastic properties of the constituent phases and most importantly, on the aspect ratio of the ceramic rod. Plotted in figure 6 is the calculated results for d_h from eq. (9) for several different aspect ratios for a PZT5H-Spurs epoxy composite. The input data can be found in reference 6. Clearly, aspect ratio of the PZT rod is an important parameter in determining the piezoelectric performance of 1-3 composites.

Shown in figure 7 is the comparison between the experimentally measured d_h for a 1-3 composite with 1% PZT volume content in spurs epoxy matrix and that calculated from equation (9). The parameters used in the calculation are listed in reference 6, and d_{33} and d_{31} were treated as fitting parameters. The agreement between the experimental result and theoretical calculation is satisfactory.

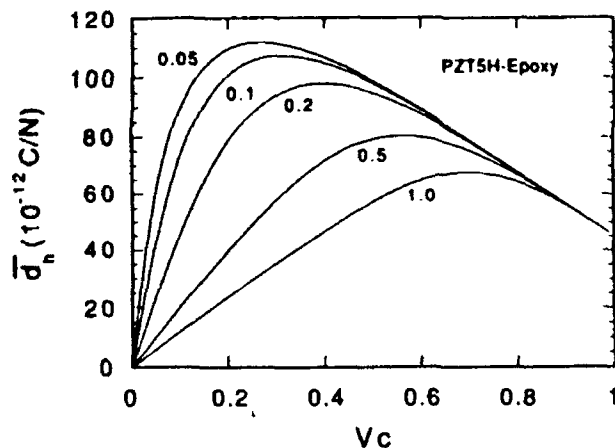


Figure 6: The hydrostatic piezoelectric constant d_h , as a function of the ceramic content at the aspect ratio of $a/L=0.05, 0.1, 0.2, 0.5$ and 1.0 for a single rod PZT5H-Epoxy 1-3 composite.

Conclusions

In general, the response of the constituent phases of a composite to an external field is not uniform spatially. By taking into account the nonuniform strain profiles in the constituent phases, the theoretical model presented in this paper can quantitatively predict the performance of these composites. Theoretical predictions agree quantitatively with the experimental results.

where V_c is the volume content of the ceramic in the composite, d_{33}^c and d_{31}^c are the piezoelectric constants of the ceramic phase, and γ_h is the stress amplification factor.⁶

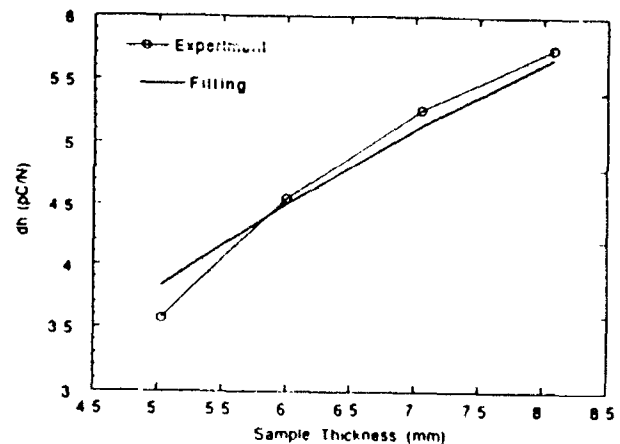


Figure 7: Thickness dependence of d_h for a 1-3 composite and the comparison with the theoretical prediction. The radius of the PZT rod is 0.405 mm.

References

- [1] Newnham, R. E., D. P. Skinner, and L. E. Cross, "Connectivity and Piezoelectric-Pyroelectric Composites," *Materials Res. Bull.*, vol 13, pp. 525-536, 1978
- [2] Gururaja, T. R., A. Safari, R. E. Newnham, and L. E. Cross, "Piezoelectric Ceramic-Polymer Composites for Transducer Applications," in *Electronic Ceramics*, ed L. M. Levinson, pp 92-128, New York: Marcel Dekker, 1987.
- [3] Smith, W. A., B. A. Auld, "Modeling 1-3 Composite Piezoelectrics: Thickness-Mode Oscillations," *IEEE Trans. on Ultrasonics, Ferro., and Freq. Control*, vol 38, pp. 40-47, 1991.
- [4] Wenwu Cao, Q. M. Zhang, and L. E. Cross, "Theoretical Study on the Static Performance of Piezoelectric Ceramic-Polymer Composites with 2-2 Connectivity," *IEEE Trans. Ultrasonics, Ferro., and Freq. Control*, in press, 1992.
- [5] Q. M. Zhang, Wenwu Cao, H. Wang, and L. E. Cross, "Characterization of the Performance of 1-3 Type Piezocomposites for Low Frequency Applications," submitted to *J. Appl. Phys.*, 1992.
- [6] Wenwu Cao, Q. M. Zhang, and L. E. Cross, "Theoretical Study on the Performance of Piezoelectric Ceramic-Polymer Composites with 1-3 Connectivity," accepted by *J. Appl. Phys.*, 1992.

APPENDIX 5

PIEZOELECTRIC TUBES AND TUBULAR COMPOSITES
FOR ACTUATOR AND SENSOR APPLICATIONS

Q. M. Zhang, H. Wang, and L. E. Cross

Materials Research Laboratory, The Pennsylvania State University
University Park, PA 16802

Abstract: The piezoelectric actuators and sensors made of tubular structure can provide a great agility of the effective response in the radial direction. For a radially poled piezoelectric tube, the effective piezoelectric constant in that direction can be tuned to be positive, zero, and negative by varying the ratio of the outer radius (R_0) to the inner radius (r_0) of the tube. For a suitable ratio of R_0/r_0 , this effective constant can also be changed in sign or set to zero by adjusting the DC bias field level for tubes made of electrostrictive materials. Therefore, one can make a piezoelectric transducer with all the effective piezoelectric tensile constants having the same sign. The end capped thin wall tubes also exhibit exceptionally high hydrostatic response and the small size of the tubular structure makes it very suitable for integration into 1-3 composite which possesses low acoustic impedance and high hydrostatic response.

I. INTRODUCTION

The recent advance in the adaptive materials and structures has put increasing demands on new materials and material structures to broaden the range of material properties provided by the conventional materials.^{1,2} The novel concept of piezocomposites is one such example which combines two or more materials with complementary properties to expand the effective properties of the composite beyond those of each individual component.^{3,4} With the existing materials, by structure modifications, one can also greatly improve the performance of devices. In this paper, we will examine the effective piezoelectric properties of a tubular structure and its composites formed from arrays of such tube for both actuating and sensing applications. For a radially poled ceramic tube, the competition between the piezoelectric d_{33} effect and d_{31} effect in the radial direction provides a convenient way to adjust the effective piezoelectric properties in that direction by changes in the tube radii. The small thickness of a thin wall tube also makes it practical to use field biased electrostrictive materials for actuators and sensors since only a low terminal DC voltage is required to produce substantial piezoelectric activities in the materials in this geometry.

II. PIEZOELECTRIC RESPONSE OF A TUBE UNDER AN ELECTRIC FIELD

When a radially poled tube is subjected to an electric field along the radial direction, on the average, the strain in the axial direction equals $d_{31} E_m$, where d_{31} is the linear piezoelectric constant and E_m is the average field in the material. The response in the radial direction, however, is complicated. In this section, the solution of the elastic equation for the tubular structure under an electric field will be presented. It will be shown that with the same applied electric field, the outer diameter (OD) (or the inner diameter (ID)) of the tube can either expand or contract depending on the ratio of the OD to ID of the tube. This

phenomenon is the direct consequence of the competition between the piezoelectric d_{33} and d_{31} effects, which have opposite sign in producing the change in the tube OD under electric field.

In analyzing the strain response of a tubular structure under an electric field, it is convenient to use the cylindrical polar coordinate system, as shown in figure 1. The symmetry of the problem requires that the ϕ -component of the displacement field $u_\phi=0$. For a thin wall tube, one can neglect the coupling terms containing both r and z in the displacement field \vec{u} and assume $\vec{u}=u_r(r)\hat{r} + u_z(z)\hat{z}$. Under this approximation, the non-

zero strain component are: $u_{rr}=\frac{\partial u_r}{\partial r}$, $u_{\phi\phi}=\frac{u_r}{r}$, and $u_{zz}=\frac{\partial u_z}{\partial z}$. The constitutive relations for

the tube, therefore, are

$$\begin{aligned} T_z &= c_{11} u_{zz} + c_{12} u_{\phi\phi} + c_{12} u_{rr} - e_{31} E \\ T_r &= c_{11} u_{rr} + c_{12} u_{\phi\phi} + c_{12} u_{zz} - e_{33} E \\ T_\phi &= c_{12} u_{zz} + c_{11} u_{\phi\phi} + c_{12} u_{rr} - e_{31} E \end{aligned} \quad (1)$$

where T_z , T_r , and T_ϕ are the stress components in the three directions, the c_{ij} are the elastic stiffness constants, the e_{ij} are the piezoelectric stress constants, and E is the applied electric field within the tube wall in the r -direction. It is well known that the electric field is not a

constant inside the tube wall and with a total voltage V applied to the tube, $E = \frac{V}{r \ln(R_0/r_0)}$

($r_0 \leq r \leq R_0$). In equations (1), we made the approximation that the tube is isotropic elastically to simplify the analysis. The effect of anisotropy will be addressed in the next section in which we discuss the hydrostatic response of end capped tubes. Both experimental data, which will be presented later in this section, and the analysis in the next section show that the errors due to the isotropic approximation are not significant.

Making use of the constitutive equation (eq. (1)) and the static equilibrium condition, we can derive the basic elastic equations for this problem⁵

$$\frac{\partial}{\partial r} \left(\frac{1}{r} \frac{\partial}{\partial r} r u_r \right) = - \frac{e_{31} E s_{11} (1+\sigma)(1-2\sigma)}{r (1-\sigma)} \quad (2)$$

$$\frac{\partial u_z}{\partial z} = \text{constant}$$

where σ is the Poisson's ratio and s_{11} is the elastic compliance. The solutions to eq. (2) are

$$u_r = ar + \frac{b}{r} + \frac{e_{31} V s_{11} (1+\sigma)(1-2\sigma)}{\ln \rho (1-\sigma)} \quad (3)$$

and $u_z = cz$

where $\rho = R_0/r_0$. a , b and c are the integration constants which can be determined from the boundary conditions: $u_{zz} = d_{31} E_m$, where E_m is the average radial electric field in the tube

($E_m = \frac{2V}{(R_0+r_0) \ln(R_0/r_0)}$), and at $r=R_0$ and r_0 , there is no external stress on the tube wall

which implies $T_r=0$ at these two boundaries. Substituting eqs. (3) into eqs. (1) and using the boundary conditions, one can get

$$a = E_m ((1-2\sigma) d_{33} - \sigma d_{31}) / (2(1-\sigma))$$

$$b = -R_0 r_0 E_m (d_{33} + \sigma d_{31}) / (2(1-\sigma)) \quad (4)$$

$$c = d_{31} E_m$$

The strain components for the tube can be obtained from eqs. (3) and (4). Here we are more interested in finding out how the tube outer diameter changes with applied electric field as the ratio of R_0/r_0 varies since in most of the applications, this is the quantity of interest. Substituting a and b from equation (4) into equation (3) for u_r and setting $r=R_0$ yield the displacement of the tube outer wall $u_r(R_0)$

$$u_r(R_0) = E_m ((R_0+r_0) d_{31} + (R_0-r_0) d_{33}) / 2$$

This equation reveals that $u_r(R_0)$ can be changed from positive to zero, and to negative by varying the ratio of R_0/r_0 .

To illustrate the advantage of using thin wall tubes for actuator applications, one can compare the piezoelectric response of a tube with a rod of radius R_0 , both of length L subjected to the same applied voltage V . For the rod, the field is applied along the axial direction and $u_{zz}=d_{33} V/L$ and $u_{rr}=d_{31} V/L$. For the tube sample, one can equivalently introduce the quantity u_r/R_0 as the effective strain in the radial direction

$$u_r(R_0)/R_0 = E_m ((1+r_0/R_0) d_{31} + (1- r_0/R_0) d_{33})/2 \quad (5)$$

Similar to a rod sample, we introduce the effective piezoelectric constants for the tube as if it were a rod poled axially,

$$u_{zz}=d_{33}^{\text{eff}} V/L \quad \text{and} \quad \frac{u_r}{R_0} = d_{31}^{\text{eff}} V/L \quad (6)$$

where L is the axial length of the tube and V is the voltage applied on the tube wall. From $u_{zz}=d_{31} E_m$ and equation (5), the effective piezoelectric constants can be deduced

$$d_{33}^{\text{eff}} = d_{31} \frac{2L}{(R_0+r_0)\ln(R_0/r_0)} \quad (7)$$

$$d_{31}^{\text{eff}} = \frac{L}{(R_0+r_0)\ln(R_0/r_0)} \left[\left(1 + \frac{r_0}{R_0}\right) d_{31} + \left(1 - \frac{r_0}{R_0}\right) d_{33} \right]$$

For thin walled tubes with L much larger than R_0 , which is the case in most of the applications, both d_{33}^{eff} and d_{31}^{eff} can be exceptionally large. This demonstrates that the tubular structure has great advantage over the regular ceramic rod for actuator applications. Besides that, by choosing $(1+r_0/R_0) |d_{31}| > (1-r_0/R_0) |d_{33}|$, the effective d_{33} and d_{31} of the tube will have the same sign. By adjusting the ratio R_0/r_0 , one can also continuously vary d_{31}^{eff} of the tube from positive to zero and to negative.

To compare with theory, the displacement field $u_r(R_0)$ and u_{zz} of a radially poled PZT-5 tube were measured using a double beam laser dilatometer.⁶ The ceramic tubes used were manufactured by Morgon Matroc, Inc., Vernitron Div. with $R_0=0.635$ mm and

$r_0=0.381$ mm. From the data acquired and using eqs (3), (4) and (5), we got $d_{33}=289$ pC/N and $d_{31}=-141.3$ pC/N for the tube material. For most of commercially available PZT materials, the ratio of d_{33}/d_{31} ranges from 2.15 to 2.3.⁷ The measured ratio here ($d_{33}/d_{31}=2.05$) is slightly below that range which we believe is the result of the approximations used in the derivation. The effective piezoelectric constants defined in eq. (6) for the tube, therefore, are $d_{33}^{eff}=-8180$ pC/N and $d_{31}^{eff}=-3220.5$ pC/N, the two coefficients have the same sign as predicted by eq. (7) and they are exceptionally large.

The small thickness of the tube wall also makes it possible to use electric field biased electrostrictive materials for the actuator application since only a small bias voltage is required here to induce substantial piezoelectric responses in the materials. In the field biased electrostrictive materials, it has been shown that the ratio of the piezoelectric constants d_{33}/d_{31} is bias field dependent.⁸ Hence, for a suitable ratio of R_0/r_0 , by tuning the DC bias field level, both sign and magnitude of d_{31}^{eff} of the tube can be varied.

III. THE HYDROSTATIC RESPONSE OF END CAPPED TUBES

The availability of small size ceramic tubes makes it attractive to integrate them into 1-3 type piezoceramic-polymer composites for large area applications and to provide more flexibility for further material property modification. Before a detailed discussion of composite properties, we will derive the expression for the hydrostatic response of end capped tubes since they are commonly used as hydrostatic sensor.⁹ As demonstrated in section II, the ratio of R_0/r_0 provides a convenient way to adjust the stress sensitivity of the sensor.

Similar to the derivations presented in the preceding section, the displacement field of a tube under hydrostatic pressure, when expressed in the cylindrical coordinate system, is $u_\phi=0$ and $\vec{u}=u_r(r) \hat{r} + u_z(z) \hat{z}$. (For an isotropic material, this is the exact form of the

displacement field equations. For a poled ceramic tube, the error in using this form of the displacement field, as will be shown later, is less than 10%.) Since the tube is capped on both ends, the pressure field is applied only to the outer surfaces of the tube, eq. (2) becomes:

$$\frac{\partial r u_r}{r \partial r} = \text{const.} \quad \text{and} \quad \frac{\partial u_z}{\partial z} = \text{const.} \quad (8)$$

The solutions to the equations are:

$$u_r = a r + b/r \quad \text{and} \quad u_z = c z \quad (9)$$

The non-zero strain components are:

$$u_{rr} = a - b/r^2, \quad u_{\phi\phi} = a + b/r^2, \quad \text{and} \quad u_{zz} = c \quad (10)$$

where a, b, and c are the integration constants which can be determined from the boundary conditions. The boundary conditions are: at $r=r_0$, $T_r = 0$; at $r=R_0$, $T_r = -p$; and at $z=0$ and $z=l$, the stress in the axial direction is $T_z = -p R_0^2 / (R_0^2 - r_0^2)$, where $-p$ is the applied hydrostatic pressure. For the purpose of comparison, we will determine the integration constants a, b, and c in eq. (9) for both an elastically isotropic tube and a piezoelectric ceramic tube. For the later tube, the constitutive relations are:

$$\begin{aligned} T_z &= c_{11} u_{zz} + c_{12} u_{\phi\phi} + c_{13} u_{rr} \\ T_r &= c_{33} u_{rr} + c_{13} u_{\phi\phi} + c_{13} u_{zz} \\ T_\phi &= c_{12} u_{zz} + c_{11} u_{\phi\phi} + c_{13} u_{rr} \end{aligned} \quad (11)$$

where c_{ij} are the elastic stiffness coefficients of the poled ceramics. Following the convention in the literature, in eq. (11), 3 refers to the poling direction (\hat{r} direction), 1 the \hat{z} direction, and 2 the $\hat{\phi}$ direction. Substituting the strain components from eq. (10) into eq. (11) and omitting the term in T_z having r dependence, one can obtain a, b, c:

$$a = \frac{-p R_0^2}{R_0^2 - r_0^2} \left[\frac{c_{13} - c_{11}}{c_{13}(c_{12} + c_{13}) - c_{11}(c_{13} + c_{33})} \right] \quad (12a)$$

$$b = \frac{-r_o^2 R_o^2 p}{R_o^2 - r_o^2 c_{33} - c_{13}} \quad (12b)$$

$$c = \frac{-p R_o^2}{R_o^2 - r_o^2} \left[\frac{c_{12} - c_{33}}{c_{13}(c_{12} + c_{13}) - c_{11}(c_{13} + c_{33})} \right] \quad (12c)$$

Therefore, the stress distribution in the tube is given by:

$$T_r = \frac{-p R_o^2}{R_o^2 - r_o^2} \left[1 - \frac{r_o^2}{r^2} \right] \quad (13a)$$

$$T_\phi = \frac{-p R_o^2}{R_o^2 - r_o^2} \left[\frac{c_{13}^2 + c_{12}^2 - c_{11}^2 - c_{12}c_{33}}{c_{13}(c_{12} + c_{13}) - c_{11}(c_{13} + c_{33})} + \frac{c_{11}c_{13}}{c_{33}c_{13}} \frac{r_o^2}{r^2} \right] \quad (13b)$$

$$T_z = \frac{-p R_o^2}{R_o^2 - r_o^2} \quad (13c)$$

A term $((c_{12}-c_{13})b/r^2)$, which is less than 7% of the total T_z , was omitted from eq. (13c). Since T_z itself is one of the boundary condition used to derive the integration constants a, b, and c and is equal to $-p R_o^2/(R_o^2 - r_o^2)$, the appearance of this extra-term in the expression for T_z derived using eqs. (11) and (12) is believed to be an error resulting from the approximation made for the displacement field for the tube under hydrostatic pressure. However, the small size of this error (less than 7%) indicates the approximation is acceptable.

From the stress distribution equations, the hydrostatic response of the tube can be calculated from the relation

$$D_3 = d_{31} T_z + d_{31} T_\phi + d_{33} T_r \quad (14)$$

where D_3 is the electric displacement in the poling direction. The value of d_h can be found by taking the average charge produced in the inner and outer surfaces of the tube wall and divided it by the outer surface area of the tube. From eq. (14):

$$d_h = \frac{1}{2} \left\{ d_{33} + \frac{R_o}{R_o - r_o} \left[1 + \left(\frac{c_{13}^2 + c_{12}^2 - c_{11}^2 - c_{12}c_{33}}{c_{13}(c_{13} + c_{12}) - c_{11}(c_{13} + c_{33})} \right) + \frac{c_{11} - c_{13}}{c_{33} - c_{13}} \frac{r_o}{R_o} \right] d_{31} \right\} \quad (15)$$

In eq. (15), we have taken the tube outer surface as the total electroded area to calculate d_h . Using the elastic stiffness coefficients for PZT-5H,⁷ for a tube with $R_0=0.635$ mm and $r_0=0.381$ mm, eq. (15) predicts $d_h = -657$ pC/N or $2.4 d_{31}$. If the radius R_0 is doubled while keeping the wall thickness the same, d_h increases to -1786 pC/N. Hence, for thin walled tubes, an exceptionally large hydrostatic response can be achieved.

Eq. (13) can be reduced to the stress field of an elastically isotropic tube by using the isotropic conditions $c_{11}=c_{33}$, $c_{12}=c_{13}$. It can be shown that the result thus obtained is the exact solution to the tube stress field and similarly d_h can be found by simplifying eq. (15) using the isotropic condition:

$$d_h = \frac{1}{2} \left(d_{33} + \frac{R_o}{R_o - r_o} \left[2 + \frac{r_o}{R_0} \right] d_{31} \right) \quad (16)$$

Using the data above for the PZT-5H tube, the value of d_h calculated from eq. (16) is found to be -594 pC/N ($2.17 d_{31}$).

Experimental measurements were performed on several PZT-5 tubes ($R_0=0.635$ mm and $r_0=0.381$ mm) with two ends sealed and radially poled (the dielectric constant ϵ for this group of samples is around 1700 at the ambient pressure). d_h was determined by the direct piezoelectric effect, i.e. by measuring the charge induced on the electrodes of a sample which is subjected to a hydrostatic pressure. d_{31} and d_{33} were measured using a double beam laser interferometer.⁶ For this group of samples, d_h ranged from -330 pC/N to -400 pC/N and d_{31} from -140 pC/N to -160 pC/N. The ratio between the experimental values of d_h and d_{31} (on average) is 2.45 which is very close to that predicted from eq. (15).

Clearly, to make a quantitative prediction of the hydrostatic response of a tubular structure, one should include the elastic anisotropy in the calculation.

In analogy to the situation discussed in the preceding section, by varying the ratio of R_0/r_0 , one can also manipulate the response of the tube to the stress field in the radial direction. Here, we will use the result just derived for the hydrostatic response of a tube as

an example. From eq. (14), the hydrostatic response of a tube comes from three terms, one is from the pressure in the axial direction and the other two from the pressure in the radial direction. The electric displacement D_3^r due to the pressure in the radial direction is

$$D_3^r = d_{31} T_\phi + d_{33} T_r$$

Using the result of eq. (13) and taking the average charge produced at the tube inner wall and outer wall, one can obtain the piezoelectric response d^r of the tube to the pressure in the radial direction

$$d^r = \frac{1}{2} \left(d_{33} + \frac{R_o}{R_o - r_o} \left[\left(\frac{c_{13}^2 + c_{12}^2 - c_{11}^2 - c_{12}c_{33}}{c_{13}(c_{13} + c_{12}) - c_{11}(c_{13} + c_{33})} \right) + \frac{c_{11} - c_{13}}{c_{33} - c_{13}} \frac{r_o}{R_o} \right] d_{31} \right) \quad (17)$$

Since d_{33} and d_{31} are opposite in sign, one can easily verify that by varying the ratio of R_o/r_o , d^r changes continuously from positive to zero, and to negative. Taking the elastically isotropic tube as an example and assuming $d_{33}/d_{31}=2.2$ in eq. (17), when $r_o/R_o=0.375$, d^r becomes zero. That is, the tube now becomes insensitive to the pressure wave in the radial direction. Similar to the actuator case, for suitable ratio of r_o/R_o , one can also change the sign of the effective radial response here by using electrostrictive materials with different DC bias field levels. This result as well as the result in the preceding section indicate that the range of the effective piezoelectric properties of the materials can be considerably broadened by using the tubular structures.

To calculate the hydrostatic figure of merit for this tubular sensor, we notice that in practice, the quantity $d_h g_h$ is a measure of the product of the charge and voltage produced in a unit volume material. For a tubular material, its effective volume is $\pi R_o^2 L$, where L is the tube length when the end capped tube is regarded as a rod with its radius equal to R_o .

The capacitance of the tube is

$$C = \frac{2\pi L \epsilon_0 \epsilon}{\ln(R_o/r_o)}$$

where ϵ is the dielectric constant of the material. Since the total charge produced by the tube is equal to $2\pi R_0 L d_h$ and the voltage is equal to this charge divided by the capacitance of the tube, the effective figure of merit for the tube is

$$d_h g_h = \frac{1}{2\epsilon\epsilon_0} \ln\left(\frac{R_0}{r_0}\right) \left(d_{33} + d_{31} \left(\frac{R_0}{R_0 - r_0} \right) \left(2 + \frac{r_0}{R_0} \right) \right)^2 \quad (18)$$

Here, we have used d_h result for an isotropic tube (eq (17)). One can easily find the equivalent expression for a elastically anisotropic tubes. Clearly, a large figure of merit can be obtained for a thin walled tube.

IV. 1-3 TUBULAR COMPOSITES

A 1-3 composite consisting of piezoelectric ceramic tubes embeded in a polymer matrix is shown schematically in figure 2. For the composite discussed here, the tubes are radially poled and are electroded on the inner and outer cylindrical surfaces, the composite is electroded on the two end faces. Hence, special arrangements are required to ensure proper electric connections between the electrodes at the tube walls and the end faces of the composite. This kind of composite can be used for large area actuator and sensor applications, as well as smart materials in where both sensor and actuator are integrated into a single structure. In this section, we only discuss the properties of the composite associated with the sensor applications.

When tubes are integrated into a 1-3 type ceramic-polymer composite, as has been demonstrated in our earlier publications, there is a stress transfer between the polymer matrix and the ceramic tubes in the z-direction,^{10,11} which is the result of the difference in the elastic constants between the two constituent phases and is through the shear force in the two phases. Due to this stress transfer, the piezoelectric response of the tube in the axial direction is enhanced. To provide a physical picture of how the hydrostatic response

of a tubular 1-3 composite changes as the elastic properties of the two constituent phases and their geometric parameters are varied, we will treat quantitatively the composite schematically drawn in figure 3. This composite corresponds to the tubular composite in the dilute limit. However, since only the polymer matrix close to the ceramic-polymer interface participates in the stress transfer, the result can also be applied to composites with finite ceramic content.

The procedure for calculating the stress transferred from the polymer phase to the ceramic rod is similar to that outlined in the earlier publications.^{10,11} Under hydrostatic pressure p , the surface displacement field u_z of the polymer phase in the z -direction should satisfy the following equation

$$\frac{2u_z}{L} = -(s_{11} + 2s_{12})p + \frac{s_{11}\mu L}{4} \left(\frac{\partial^2 u_z}{\partial r^2} + \frac{\partial u_z}{r \partial r} \right) \quad (19)$$

where p is the hydrostatic pressure, s_{ij} is the elastic compliance of the polymer phase, μ is the shear modulus of the polymer phase, and L is the thickness of the composite in the z -direction. The solution to eq. (19) is the zeroth-order Hankel function $K_0(\rho)$ and

$$\frac{2u_z}{L} = -\frac{(1-2\sigma)p}{Y} + A K_0(r/\xi) \quad (20)$$

where A is the integration constant and $\xi = L/(2\sqrt{2Y/\mu})$, defines the strain decay length in the polymer phase. In eq. (20), we have made use of the relationships $s_{12} = -\sigma s_{11}$ and $Y = 1/s_{11}$, where Y and σ are the Young's modulus and the Poisson's ratio of the polymer, respectively. The total force f transferred from the polymer phase to the ceramic tube is, therefore

$$f = Y \int_{r_0}^{\infty} 2\pi r A K_0(r/\xi) dr$$

Two boundary conditions are needed to determine f : the first is that at the ceramic tube-polymer interface, the z -component of the strain in the two phases should be equal, and the

second is the relationship between the z-component of the strain in the ceramic tube and the stress field

$$u_{zz} = -\frac{pR_0^2(1-\sigma^c)s_{11}^c}{R_0^2-r_0^2} + \frac{fs_{11}^c}{\pi(R_0^2-r_0^2)} \quad (21)$$

where s_{11}^c and σ^c are the elastic compliance and the Poisson's ratio of the ceramic tube respectively. Eq. (21) can be derived following the procedure outlined in the preceding section. Hence, the amount of stress transferred from the polymer matrix to the ceramic tube is

$$\frac{f}{\pi A_0} = -\frac{pR_0^2}{A_0} \left(\frac{A_0(1-2\sigma)/(R_0^2 Y s_{11}^c) - (1-2\sigma^c)}{1 + K_0(\rho_0)A_0 / (2K_1(\rho_0)Y s_{11}^c R_0 \xi)} \right) \quad (22)$$

where $A_0=(R_0^2-r_0^2)$, $\rho_0=R_0/\xi$, and $K_1(\rho)$ is the first order Hankel function. Since the polymer phase is subjected to a hydrostatic pressure, the Poisson's ratio effect causes the reduction of the effective pressure at the polymer faces from $-p$ to $-p(1-2\sigma)$. As shown in eq. (22), this reduces the stress transfer from the polymer phase to the ceramic tube. To increase the stress transfer, one should choose polymers with small Poisson's ratio. The total stress in the axial direction of the tube is

$$\begin{aligned} T_z &= -\frac{pR_0^2}{A_0} \left(1 + \frac{A_0(1-2\sigma)/(R_0^2 Y s_{11}^c) - (1-2\sigma^c)}{1 + K_0(\rho_0)A_0 / (2K_1(\rho_0)Y s_{11}^c R_0 \xi)} \right) \\ &= -\frac{pR_0^2}{A_0} \gamma \end{aligned} \quad (23)$$

where γ is introduced as the stress amplification factor. In figure 4, we plot γ as a function of the aspect ratio R_0/L for a 1-3 tubular composite made of PZT-5H tube with $R_0=0.635$ mm and $r_0=0.381$ mm and spurs epoxy.¹² Apparently, for thin and long tubes, the stress amplification factor is large. This result is similar to that obtained earlier for 1-3 composites made from ceramic rods embedded in a polymer matrix.^{10,11}

Using the results from section III and equation (23), one can write down the effective hydrostatic piezoelectric strain coefficient for 1-3 tubular composites

$$d_h^{\text{eff}} = \frac{L}{R_0} v_c \left(d_{33} + \frac{R_0}{R_0 - r_0} \left(1 + \gamma + \frac{r_0}{R_0} \right) d_{31} \right) \quad (24)$$

where v_c is the volume content of the ceramic tubes in the composite which is defined as $v_c = \pi R_0^2/a$, and a is the unit cell area of the composite. For a composite with low ceramic volume content, γ in eq. (22) is equal to that in eq. (24). With increased volume content, the dependence of γ on the material properties of the constituent phases will become more complicated and one may not be able to derive an analytical expression for γ except in some special cases. In this paper, we will not pursue this further and only point out that in the composite, there is always a stress transfer between the two phases ($\gamma > 1$). The general rule for increasing stress transfer is basically the same as that for the dilute composite case.

In the limit of $v_c \Rightarrow 1$, eq. (24) is reduced to that for a single tube when regarded as a rod with the similar dimensions

$$d_h^{\text{eff}} = \frac{L}{R_0} \left(d_{33} + \frac{R_0}{R_0 - r_0} \left(2 + \frac{r_0}{R_0} \right) d_{31} \right) \quad (25)$$

Eq. (16) can be converted to eq. (25) by using the area of the tube end (πR_0^2) as the effective electrode area instead of the area of the tube outer wall. Similarly, one can also derive the effective hydrostatic figure of merit for 1-3 tubular composites

$$d_h^{\text{eff}} g_h^{\text{eff}} = \frac{v_c}{2\epsilon\epsilon_0} \ln\left(\frac{R_0}{r_0}\right) \left(d_{33} + \frac{R_0}{R_0 - r_0} \left(1 + \frac{r_0}{R_0} + \gamma \right) d_{31} \right)^2 \quad (26)$$

As $v_c \Rightarrow 1$ ($\gamma \Rightarrow 1$), the result is reduced to that for a single tube sensor (eq. (18)).

For the comparison, in table 1, we present the experimental values of the hydrostatic response of an end capped ceramic tube, a 1-3 composite with air filled capped ceramic tubes (air backing), and a 1-3 composite with epoxy backed ceramic tubes. The two 1-3 composites have ceramic tube volume content of 23.3 % . The dimensions of the tubes are: $R_0=0.635$ mm, $r_0=0.381$ mm, and $L=9$ mm. The polymer matrix was made of spurs

epoxy. For the data in the table, d_{31} was calculated using eq. (25) for a ratio $R_0/L=0.07$ where the ratio $d_{33}/d_{31}=2.2$ is used. From this d_{31} , γ was calculated from eq. (26). Clearly, the γ value here is much smaller than that shown in figure 4. One of the reasons is that figure 4 is for the composite in the dilute limit. The values of γ for composites with finite ceramic content should be smaller. The imperfect stress transfer between the two phases and the depoling effect of the tubes during the epoxy curing may also be responsible for this reduction of γ . Although the data in table I show that the hydrostatic responses of the composites tested are not as high as that of the single tube, the difference is not very large. As the volume content of ceramic tubes and other parameters in a composite are varied, the effective hydrostatic figure of merit for 1-3 tubular composites will change. Under optimum conditions, one would expect that $d_h^{eff}g_h^{eff}$ for a tubular 1-3 composite will exceed that of a single tube. Further experimental and theoretical work is required to address this issue. It is significant that the figure of merit of 1-3 tubular composites is much higher than that of 1-3 composites using ceramic rods.¹¹

If there were no stress transfer from the polymer phase to the ceramic tubes in these tubular composites, one would find for this 1-3 composite $d_h^{eff} = 3339$ pC/N and $d_h^{eff}g_h^{eff} = 2353 \times 10^{-15} \text{m}^2/\text{N}$, values much smaller than those listed in table I. That these values are much smaller clearly demonstrates the importance of the stress transfer between the two phases in a 1-3 composite.

One interesting feature from table I is that the hydrostatic response of the 1-3 tubular composite with ceramic tubes having epoxy backing does not differ significantly from that of the composite with tubes having air backing. That is, the presence of epoxy inside a tube does not change the stress distribution in the tube wall significantly except to transfer stress in the z direction. This can be understood because the elastic moduli of the ceramic tube are much higher than those of epoxy. As a result, the ceramic tube wall shields the epoxy

inside the tube from seeing the pressure in the radial direction. Conversely, the epoxy inside the tube does not exert significant amount of stress to the ceramic tube wall in the radial direction. Therefore, the epoxy filled inside of a tube provides an effective way of enhancing mechanical strength without reducing the hydrostatic response of the composite significantly.

V. SUMMARY AND ACKNOWLEDGEMENT

In this paper, the effective piezoelectric responses of the tubular structures and composites including them were evaluated both theoretically and experimentally. When used as actuators, the effective piezoelectric constant in the radial direction of a tube can be changed from positive to zero and to negative by adjusting the ratio of R_0/r_0 for piezoelectric materials or the DC bias field for electrostrictive materials. Therefore, the effective piezoelectric constants along the axial direction and the radial direction can both have the same sign. For the sensor applications, the two ends sealed tube exhibits exceptionally high hydrostatic response and analogues to the situation of actuators, the pressure response in the radial direction can be adjusted by the ratio R_0/r_0 for piezoelectric materials or the DC bias field for electrostrictive materials. For large area applications, these tubes can be readily integrated into 1-3 composite structures which provide low acoustic density and high piezoelectric activity. The effectiveness of the stress transfer between the polymer phase and the ceramic tube in 1-3 composite makes it possible to fill the inside of the ceramic tube with epoxy which increases the mechanical strength of the tubular structure without significantly reducing the piezoelectric response of the composite.

The authors wishes to thank Drs. J. Powers and A. O. Sykes for many stimulating discussions. The technical assistance of Mr. H. Chen is greatly appreciated. This work was supported by the Office of Naval Research.

REFERENCES:

1. R. E. Newnham and G. R. Ruschan, *J. Am. Ceram. Soc.* **74**, 463 (1991).
2. R. E. Newnham, Q. C. Xu, S. Kumar, and L. E. Cross, *Ferro.* **102**, 259 (1990).
3. R. E. Newnham, D. P. Skinner, and L. E. Cross, *Mat. Res. Bull.* **13**, 525 (1978).
4. W. A. Smith, *Proc. 1990 IEEE Ultrasonics Symposium*, 145 (1990).
5. L. D. Landau and E. M. Lifshitz, "Theory of Elasticity" (Pergamon Press, 1986).
6. Q. M. Zhang, S. J. Jang, and L. E. Cross, *J. Appl. Phys.* **65**, 2807 (1989).
7. See the data sheet of Morgan Matroc, Inc., Vernitron Div.
8. D. J. Taylor, D. Damjanovic, A. S. Bhalla, and L. E. Cross, Annual Report of the Materials Research Laboratory, The Pennsylvania State University (1991).
9. R. A. Langevin, *J. Acoust. Soc. Am.* **26**, 421 (1954); "Handbook of Hydrophone Element Design Technology", NUSC Technical Document 5813 (1978).
10. Q. M. Zhang, Wenwu Cao, H. Wang, and L. E. Cross, to be published in *J. Appl. Phys.* (Feb. 1993).
11. Wenwu Cao, Q. M. Zhang, and L. E. Cross, to be published in *J. Appl. Phys.* (Dec. 1992).
12. The data used are: $Y=3.1 (10^9 \text{ N/m}^2)$, $\mu=1.148 (10^9 \text{ N/m}^2)$, and $\sigma=0.35$ for spurs epoxy (from C. G. Oakley, Ph. D. Thesis, The Pennsylvania State University, 1991); $s_{11}^c=1.64 (10^{-11} \text{ m}^2/\text{N})$, and $\sigma=0.31$ (ref. 7).

Table I Hydrostatic properties of the end capped tube and 1-3 tubular composites

	ϵ	d_h^{eff} (pC/N)	$d_h^{\text{eff}} g_h^{\text{eff}}(10^{-15}\text{m}^2/\text{N})$	d_{31} (pC/N)	γ
End capped tube	2,945	-14,330	10,000	-235	1
Composite (air backing)	2,922	-5,502	6,389	-235	2.11
Composite (epoxy backing)	2,944	-4,970	5,172	-235	

FIGURES CAPTIONS:

Figure 1: Schematic drawing of a radially poled ceramic tube with outer radius R_0 and inner radius r_0 , length L . The electric field is applied on the tube wall along the radial direction.

Figure 2: Schematical drawing of 1-3 tubular composite where the ceramic tubes are embedded in a polymer matrix. The ceramic tubes are either end capped or tube inside filled with epoxy.

Figure 3: A single tube 1-3 composite. The ceramic tube is end capped.

Figure 4: The stress amplification factor γ (eq. (23)) for the composite drawn in figure 3 as a function of the aspect ratio R_0/L of the ceramic tube with PZT-5H ceramic tube and spurs epoxy.

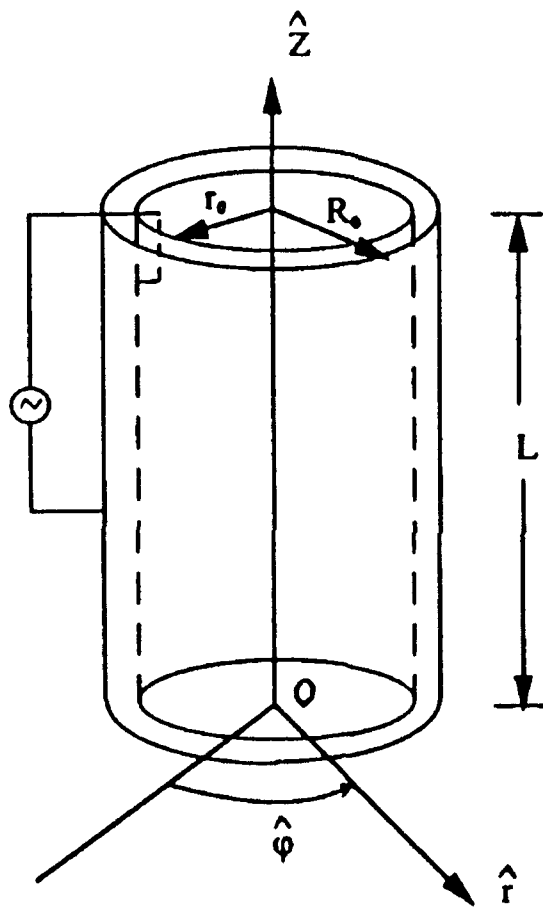
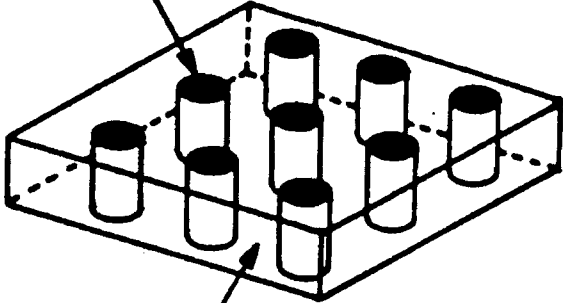


Fig. 1

Ceramic Tubes



Polymer Matrix

Fig 2

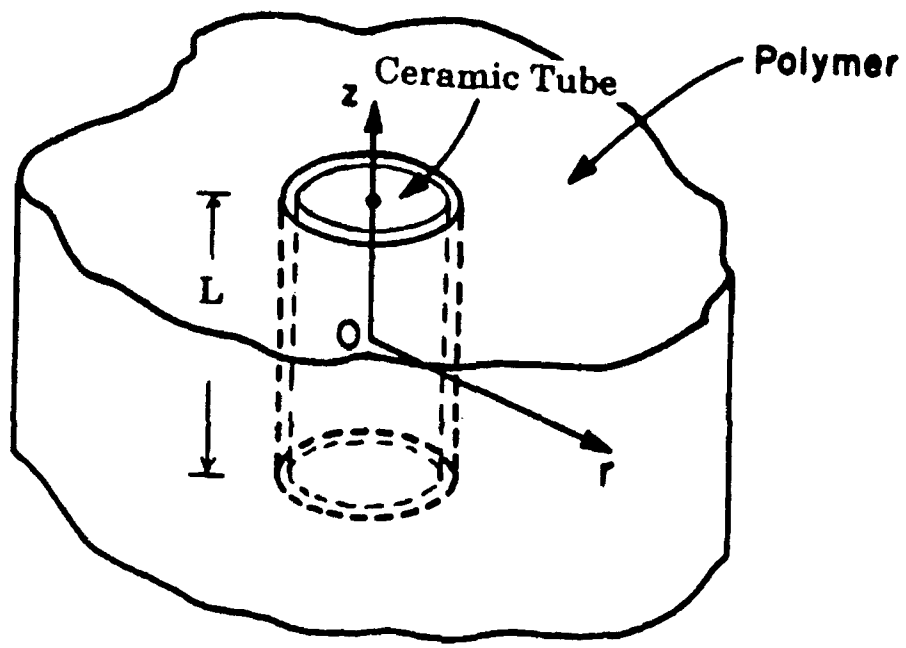


Fig. 3

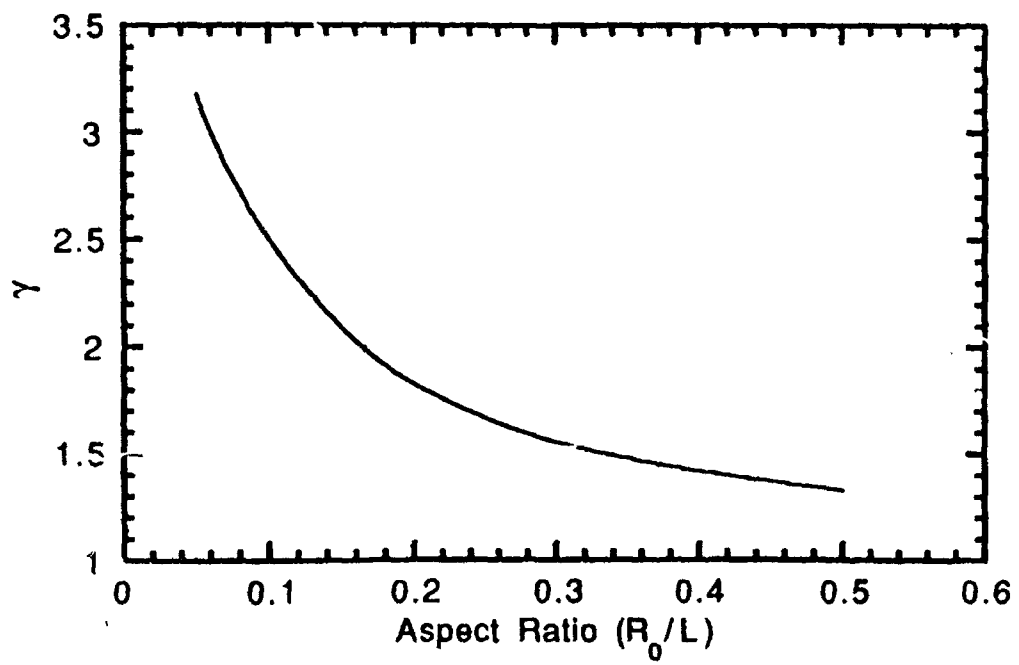


Fig. 4